inorganics

MDPI

Article

Copper Complexes of Silicon Pyridine-2-olates RSi(pyO)$_3$ (R = Me, Ph, Bn, Allyl) and Ph$_2$Si(pyO)$_2$

Anne Seidel [1], Robert Gericke [2], Erica Brendler [3] and Jörg Wagler [1,*]

[1] Institute of Inorganic Chemistry, TU Bergakademie Freiberg, D-09596 Freiberg, Germany
[2] Institute of Resource Ecology, Helmholtz-Zentrum Dresden-Rossendorf eV, D-01328 Dresden, Germany
[3] Institute of Analytical Chemistry, TU Bergakademie Freiberg, D-09596 Freiberg, Germany
* Correspondence: joerg.wagler@chemie.tu-freiberg.de; Tel.: +49-3731-39-4343

Abstract: The organosilicon pyridine-2-olates **1a**–**1d** (RSi(pyO)$_3$, R = Me (**a**), Ph (**b**), Bn (**c**), Allyl (**d**); pyO = pyridine-2-olate) may serve as tripodal ligands toward CuCl with formation of complexes of the type RSi(μ^2-pyO)$_3$CuCl (**2a**–**2d**). In addition, for R = Allyl, formation of the more stable isomer **2d′** (κO-pyO)Si(μ^2-pyO)$_2$(μ^2-Allyl)CuCl was observed. In the presence of dry air (as a source of oxygen), reactions of **1a**–**1d** and CuCl afforded Cu(II) complexes RSi(μ^2-pyO)$_4$CuCl (**3a**–**3d**); **3a**–**3c** in good yield, and **3d** only as a side product. Reaction of Ph$_2$Si(pyO)$_2$ (**4**) and CuCl in equimolar ratio afforded, depending on reaction conditions, a series of (CuCl)$_n$-ladder-type oligonuclear Cu(I) complexes Ph$_2$Si(μ^2-pyO)$_2$(CuCl)$_n$(μ^2-pyO)$_2$SiPh$_2$ (n = 2 (**5^2**), 3 (**5^3**), 4 (**5^4**)). In all of the above compounds, the pyO group is Si–O bound and, in the case of μ^2 coordination, Cu–N bound. All new compounds (**1c**, **1d**, **2b**, **2c**, **2d**, **2d′**, **3b**, **3c**, **3d**, **5^2**, **5^3**, **5^4**) were characterized by single-crystal X-ray diffraction, and further characterization includes solution ^{1}H, ^{13}C, ^{29}Si NMR spectroscopy (**1c**, **1d**, **2b**, **2c**, **2d′**, **5^3**, **5^4**), solid-state ^{29}Si (**2b**, **2c**, **2d′**, **5^3**, **5^4**) and ^{63}Cu NMR spectroscopy (**2c**, **2d′**) as well as computational analyses of the isomerization of the couple **2d**, **2d′**.

Keywords: allyl complex; 2-hydroxypyridine; hypercoordination; ^{63}Cu NMR spectroscopy; organosilanes; paddlewheel complex; quantum chemical calculations; X-ray diffraction

check for updates

Citation: Seidel, A.; Gericke, R.; Brendler, E.; Wagler, J. Copper Complexes of Silicon Pyridine-2-olates RSi(pyO)$_3$ (R = Me, Ph, Bn, Allyl) and Ph$_2$Si(pyO)$_2$. *Inorganics* **2023**, *11*, 2. https://doi.org/10.3390/inorganics11010002

Academic Editor: László Kótai

Received: 6 December 2022
Revised: 15 December 2022
Accepted: 16 December 2022
Published: 21 December 2022

1. Introduction

The facets of silicon transition metal (TM) coordination chemistry span a wide range of research fields because of the variety of binding modes encountered. Figure 1 gives some illustrative examples. Low-valent silicon species such as silylenes (in **I** [1]), intramolecularly donor-stabilized silylenes (in **II** [2]) and others (e.g., in **III** [3]) with their Si-located lone pair may act as lone pair donor ligands in the TM coordination sphere. In terms of agostic interaction, Si–Si bonds of tetravalent silicon compounds (such as disilanes, compound **IV**) may also serve as electron pair donors toward d-block elements [4]. Tetravalent silicon species may give rise to a wide range of silyl TM complexes, in which the Si atom has coordination number 4 (e.g., compounds **V** [5] and **VI** [6]). Bridging coordination of silyl anions with two or more TM atoms (e.g., in **VII** [5], **VIII** [7], **IX** [8], **X** [9]) is one way of achieving higher Si coordination numbers. Furthermore, the Lewis acidic Si site in some tetravalent silicon compounds may serve as a lone pair acceptor toward electron rich TM sites, thus furnishing higher-coordinate tetravalent Si compounds (e.g., Si coordination numbers 5 and 6) with formally dative TM→Si bond in the Si coordination sphere. Hence, silicon in Si–TM-compounds covers the full range of L-, X-, Z-type ligand characteristics [10].

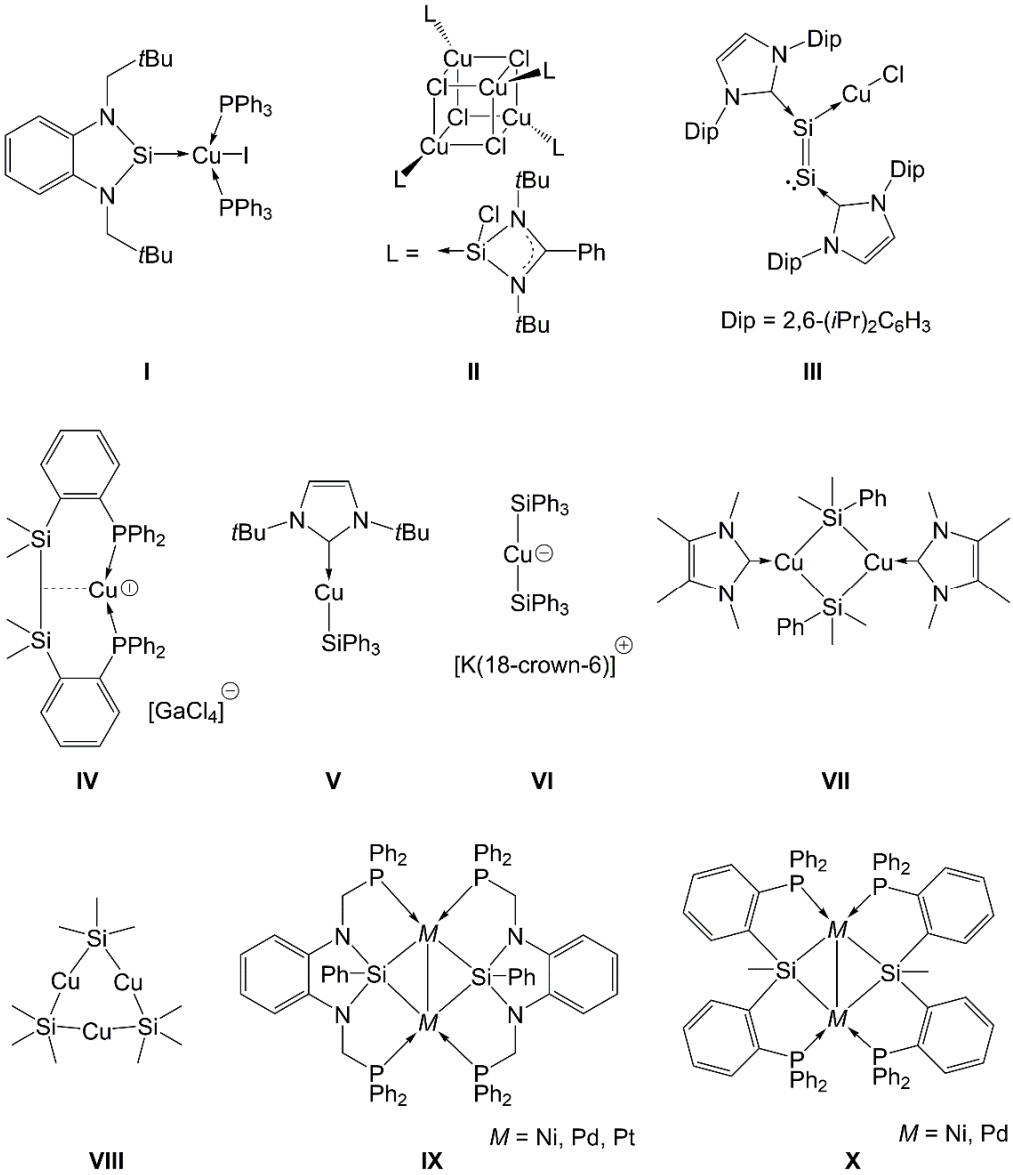

Figure 1. Selected examples of Si-Cu (**I**–**VIII**) and other Si-TM compounds (**IX**,**X**). For reasons of clarity of presentation, formal lone pair donation by L-type ligands (such as phosphanes, carbenes and silylenes) is indicated by a dative bond arrow, whereas X-type bonds (for example of silyl groups, regardless of two- or multi-center bonding thereof) are indicated by a regular bond dash.

Whereas higher-coordinate silicon compounds have fascinated chemists for many decades [11–13], TM→Si coordination chemistry represents a special and rather young topic of the coordination chemistry of higher-coordinate silicon compounds. Figure 2 illustrates examples of this class of compounds. The utilization of buttressing ligands was key to support weak attractive d^{10}-TM→Si interactions and allowed Grobe et al. to observe $^{3}J(^{31}P\text{-}^{19}F)$ coupling in NMR spectra of compound **XI** [14]. Some further examples of related complexes have been reported by the same group [15,16]. In these compounds, crystallographic analyses revealed TM–Si-distances slightly below the sum of the van der Waals radii. Over the course of the past two decades, further buttressing ligand systems have given rise to the successful preparation of a greater variety of higher-coordinate Si complexes with a TM→Si motif (e.g., compounds **XII** [17], **XIII** [18], **XIV** [19] and **XV** [20]). In some cases, TM–Si bond lengths approach the sum of covalent radii. A common feature of the buttresses used is their 1,3-ambidentate donor nature. One donor site is designed to bind to Si (as a kinetically inert Si–C bond or as a rather hard donor anion), whereas the

second site represents a rather soft donor, thus being more attractive toward late transition metals. Last but not least, the chelate effect of the ambidentate group (formation of a four-membered chelate ring) is likely to be over-compensated by the advantage of formation of a five-membered ring system when including an additional atom (i.e., a TM atom). Our recent studies, which utilized pyridine-2-olate as a buttressing motif in silane MeSi(pyO)$_3$ (**1a**), gave access to a Cu(I) complex MeSi(μ^2-pyO)$_3$CuCl (**2a**) in a deliberate manner. Furthermore, oxidative decomposition (upon access of traces of air) gave rise to the formation of small amounts of Cu(II) compound MeSi(μ^2-pyO)$_4$CuCl (**3a**), X-ray crystallographic analysis of which delivered the first proof of Cu(II)→Si coordination [20]. In the current study, we address tasks which arose from findings in this pioneering work: (1) variation of the hydrocarbyl substituent *R* in Cu(I) compounds of the type *R*Si(μ^2-pyO)$_3$CuCl and exploration of a route toward deliberate synthesis of Cu(II) compounds of type *R*Si(μ^2-pyO)$_4$CuCl to elucidate potential influence of the *R*–Si bond on the *trans*-disposed Cu→Si coordination, and (2) replacing one pyO buttress by another hydrocarbyl group to elucidate the influence of the more open system on the Cu···Si atom distance.

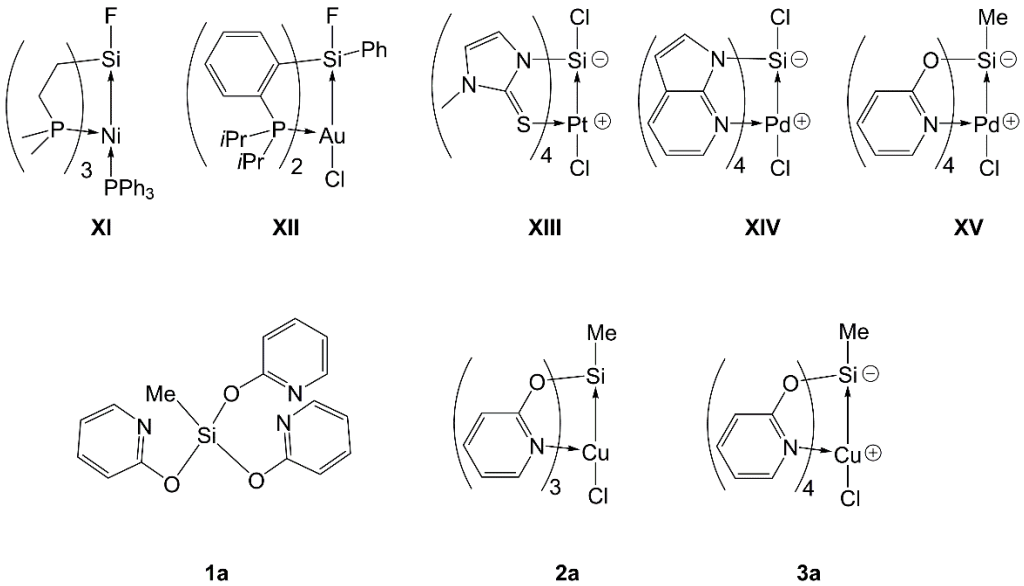

Figure 2. Selected examples of penta- and hexacoordinate Si compounds, which feature a TM atom as a formal lone pair donor in the Si coordination sphere (**XI**–**XV**) and compounds which serve as the starting point for the current study (compounds **1a**–**3a**). For reasons of clarity of presentation, formal lone pair donation by L-type ligands (such as phosphanes) is indicated by a dative bond arrow, whereas X-type bonds (for example to alkyl groups) are indicated by a regular bond dash. Formal charges are included where necessary. Note: For the molecules which feature ambidentate buttressing ligands with both donor atoms involved in π-delocalized systems, further resonance forms may be drawn.

2. Results and Discussion

2.1. Syntheses and Characterization of Cu(I) Compounds RSi(μ^2-pyO)$_3$CuCl

2.1.1. Syntheses of *R*Si(μ^2-pyO)$_3$CuCl

In studies of silatranes of the type *R*Si(OCH$_2$CH$_2$)$_3$N, the Si-bound hydrocarbyl substituent exerts influence on the through-cage N→Si dative bond. For silatranes with *R* = Me, Ph (two modifications), Allyl, Si-N-distances of 2.16 [21], 2.16, 2.13 [22,23] and 2.14 Å [24], respectively, were found. With higher electronegativity of the hydrocarbyl group, a shorter *trans*-disposed N–Si bond is observed. Thus, in order to probe the response of the *trans*-disposed potential donor atom (Cu(I) in our study), the literature example silane **1a** (*R* = Me) was supplemented by silanes *R*Si(pyO)$_3$ with R = Ph (**1b**) [25], Bn (**1c**) and Allyl (**1d**). (Note: For this study we decided to vary the Si-bound substituent within hydrocarbyl groups

only as other substituents, which are less kinetically inert at Si, may undergo substituent scrambling with pyO groups as shown for the pyridine-2-olate/-2-thiolate system [26].) Syntheses of **1a** [20] and **1b** [25] are reported in the literature, and silanes **1c** and **1d** were prepared in an analogous manner (Scheme 1). Their synthesis protocols, ^{1}H, ^{13}C, ^{29}Si NMR data as well as molecular structures (determined by single-crystal X-ray diffraction, see Table A1) are included in the Supplementary Materials.

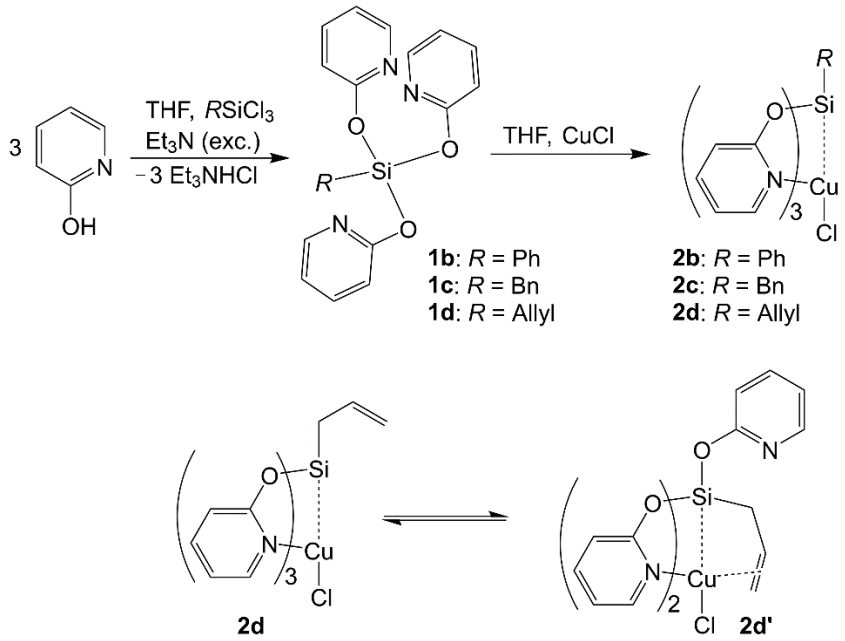

Scheme 1. Generic scheme of the syntheses of silanes *R*Si(pyO)$_3$, (**1b** [25], **1c**, **1d**) and of Cu(I) complexes thereof (**2b**–**2d**), as well as isomerization of **2d** into **2d′**.

As for the conversion of **1a** and CuCl in THF with formation of **2a** [20], the analogous reactions of silanes **1b**, **1c** and **1d** afforded the desired CuCl-complexes **2b**, **2c** and **2d**, respectively (Scheme 1). Compounds **2b** (upon diffusion of *n*-pentane into the THF solution) and **2c** (from the reaction mixture in THF) crystallized within a few days and were isolated in good yields. Compound **2d**, however, initially separated as an oil (upon diffusion of *n*-pentane into the THF solution), which turned into a yellow crystalline solid of **2d** (a crystal of which was manually extracted for XRD analysis, see Section 2.1.2). Upon further storage in the presence of the supernatant, the yellow solid recrystallized spontaneously to give colorless crystals of isomer **2d′** (see Sections 2.1.3 and 2.1.4). Further attempts at repeated syntheses of **2d** failed to give solid **2d** but afforded either an oily product or crystals of isomer **2d′**. Thus, solid-state characterization of **2d** is limited to single-crystal XRD. For further characterization in solution (see Section 2.1.5), **2d′** was used.

2.1.2. Molecular Structures of *R*Si(μ^2-pyO)$_3$CuCl (*R* = Me (**2a**), Ph (**2b**), Bn (**2c**), Allyl (**2d**))

The syntheses of compounds **2b**, **2c** and **2d** (the latter by chance) afforded crystals of the respective compound which were suitable for single-crystal X-ray diffraction analysis (Tables A1 and A2, Figure 3). Compound **2b** crystallized as a THF solvate (**2b**)$_2$·THF, the other two compounds without a solvent of crystallization. In principle, their molecular structures resemble that of pioneer **2a** [20], i.e., a cage formed by three pyO buttresses (Si–O- and Cu–N-bound) with the bridgehead atoms and their next substituent (C–Si···Cu–Cl) in a rather linear arrangement. For comparison, selected sets of corresponding interatomic distances and angles of **2b**, **2c** and **2d** are listed in Table 1.

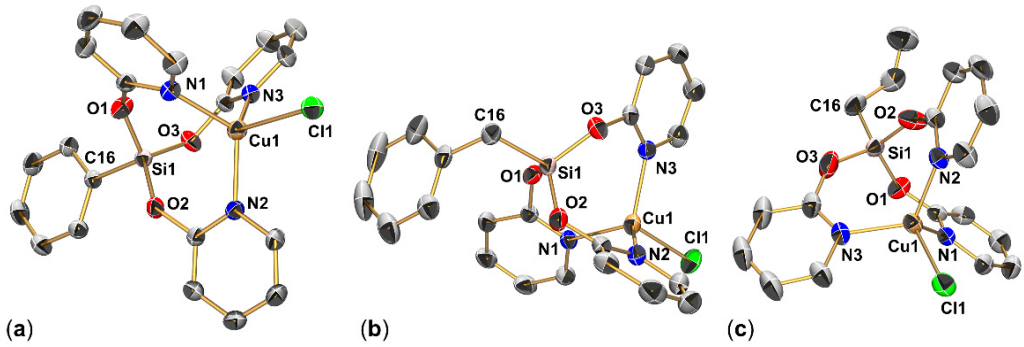

Figure 3. Molecular structures of (**a**) **2b** (in the crystal structure of the solvate $(\mathbf{2b})_2$·THF), (**b**) **2c** and (**c**) **2d** with thermal displacement ellipsoids at the 50% probability level and labels of selected non-hydrogen atoms. Selected interatomic distances and angles are listed in Table 1. For compound **2d**, only the predominant part (site occupancy 0.9) of the disordered molecule is depicted. Hydrogen atoms are omitted for clarity.

Table 1. Selected atom distances (Å) and bond angles (deg) in compounds **2b**, **2c** and **2d** in their crystal structures (as well as some corresponding parameters of one molecule of **2a** [20], the crystal structure of which features two independent molecules).

	2a	**2b**	**2c**	**2d**
Si1–O1	1.626(2)	1.633(2)	1.628(2)	1.621(2)
Si1–O2	1.629(2)	1.625(2)	1.626(2)	1.613(2)
Si1–O3	1.618(2)	1.638(2)	1.635(2)	1.612(2)
Si1–C16	1.834(3)	1.841(2)	1.855(3)	1.845(2)
Cu1–N1	2.038(2)	2.060(2)	2.037(2)	2.061(2)
Cu1–N2	2.039(2)	2.016(2)	2.049(2)	2.033(2)
Cu1–N3	2.023(2)	2.055(2)	2.073(2)	2.021(2)
Cu1–Cl1	2.361(1)	2.359(1)	2.334(1)	2.349(1)
Cu1···Si1	3.204(1)	3.211(1)	3.227(1)	3.196(1)
O1–Si1–O2	111.41(13)	113.18(9)	112.21(10)	110.99(12)
O1–Si1–O3	113.91(12)	108.96(9)	109.94(10)	111.99(13)
O2–Si1–O3	111.89(12)	113.92(9)	110.54(11)	114.26(14)
N1–Cu1–N2	112.39(8)	115.97(7)	111.40(9)	108.02(11)
N1–Cu1–N3	113.67(8)	103.62(7)	111.64(8)	113.16(11)
N2–Cu1–N3	114.46(8)	119.47(7)	113.13(9)	118.75(12)
Cl1–Cu1···Si1	177.35(2)	179.13(2)	177.70(3)	179.60(2)
Cu1···Si1–C16	177.55(13)	174.58(7)	174.01(9)	178.09(10)

In principle, bond lengths of corresponding bonds are very similar within this set of four related compounds. The slightly shorter Si–O bonds in **2d** are simulated by the disorder of the $AllylSiO_3$ moiety in the crystal structure (unresolved disorder effects reflected in the rather large thermal displacement ellipsoids of the O atoms). Interestingly, the Cu···Si distances are also very similar. They vary within a very narrow range (0.03 Å) and do not show any systematic trend with respect to the different Si-bound hydrocarbyl substituents. Within the groups of O–Si–O and N–Cu–N angles, however, noticeable variability is observed. Whereas in **2c** both sets span a rather narrow range (O–Si–O 109.9(1)–112.2(1)°, N–Cu–N 111.4(1)–113.1(1)°), the different N–Cu–N angles in **2b** (103.6(1)–119.5(1)°) indicate flexibility of these cage structures, especially in the Cu coordination sphere. With respect to the distortion of the tetrahedral Cu coordination sphere, the geometry index τ_4' [27] (**2a**: 0.93; **2b**: 0.87, **2c**: 0.95; **2d**: 0.89) also reflects noticeable differences between these related molecules in their solid-state structures. ($\tau_4' = [(\beta - \alpha)/(360° - \theta)] + [(180° - \beta)/(180° - \theta)]$ with α, β being the two greatest valence angles, $\beta > \alpha$, θ = ideal tetrahedral angle).

2.1.3. Molecular Structure of (κO-pyO)Si(μ^2-pyO)$_2$(Allyl)CuCl (**2d′**)

Compound **2d′** crystallizes in the triclinic space group $P\bar{1}$ with one molecule in the asymmetric unit (Figure 4, Table A2). The Cu···Si distance (ca. 3.3 Å) is similar to that in compounds **2a**, **2b**, **2c** and **2d**. The sum of angles around the Cu-capped tetrahedral face at Si1 (spanned by O1, O2, C16) amounts to 335.3°, thus exhibits some widening with respect to an ideal tetrahedral face. Slightly more widening, however, is observed for the face spanned by O2, O3, C16 (sum of angles 337.1°), caused by N3, which caps this face. The Cu coordination sphere can be interpreted as highly distorted pseudo-tetrahedral (with respect to the entity C17C18 occupying one ligand site), which is close to trigonal-pyramidal. With respect to the latter geometry, the ligand sites Cl1, N1 and (C17=C18) represent the base (the *cis*-angles about Cu1 spanned by those atoms amount to 352.6°), N2 the apex with N2-Cu1-X angles (X = N1, Cl1, C17, C18) ranging from 95.3 to 104.0°. The different coordination sites occupied by N1 and N2 are reflected by the different Cu–N bond lengths, with Cu1–N2 being 0.3 Å longer. Both the release of donor atom N3 in favor of Cu-allyl-coordination and the positioning of the olefinic donor entity (C17=C18) in the basal trigonal coordination plane while donor site N2 occupies a more distant axial coordination site speak for allyl groups as competitive donor arms with respect to pyridine-2-olate groups.

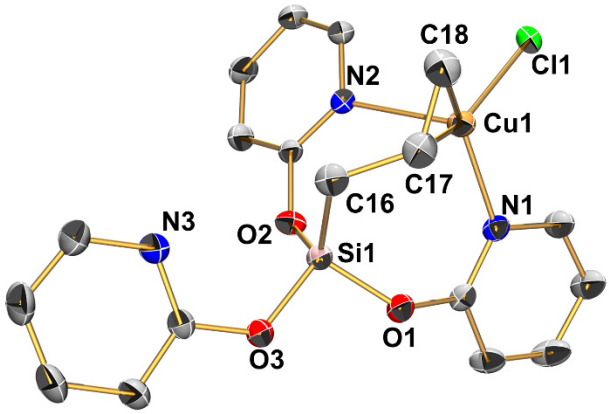

Figure 4. Molecular structure of **2d′** with thermal displacement ellipsoids at the 50% probability level and labels of selected non-hydrogen atoms. Hydrogen atoms are omitted for clarity. Selected interatomic distances (Å) and angles (deg): Cu1–Cl1 2.270(1), Cu1···Si1 3.302(1), Cu1–N1 2.047(2), Cu1–N2 2.347(2), Cu1–C17 2.095(2), Cu1–C18 2.077(2), Si1–O1 1.638(2), Si1–O2 1.637(2), Si1–O3 1.642(2), Si1···N3 2.852(2), Si1–C16 1.847(2), C16–C17 1.504(3), C17–C18 1.365(3), O1–Si1–O2 106.83(7), O1–Si1–O3 97.87(7), O2–Si1–O3 107.06(7), O1–Si1–C16 113.37(9), O2–Si1–C16 115.10(8), Cl1–Cu1–N1 102.05(5), Cl1–Cu1–N2 95.29(4), N1–Cu1–N2 104.01(6).

In principle, η^2-coordination of an allylic C=C bond to Cu(I) is a known motif. Crystallographic characterization of Cu(I) halide complexes of allyl silanes, however, is limited to few examples, a CuCl complex of Si(Allyl)$_4$ [28] and a CuI complex of Me$_2$Si(Allyl)(2-py), which forms dimer [Me$_2$Si(μ^2-2-py)(μ^2-Allyl)Cu(μ^2-I)$_2$Cu(μ^2-2-py)(μ^2-Allyl)SiMe$_2$] [29]. In the latter case, a 2-pyridyl group serves as an additional bridging ligand between Si and Cu, and the Cu atom is situated in a pseudo-tetrahedral (N,C=C,I,I)-coordination sphere. This pyridyl-supported CuI-complex of an allyl silane was found to be an allyl transfer reagent when reacted with benzaldehyde in the presence of CsF, whereas a mixture of Me$_3$Si(Allyl), CuI, Benzaldehyde and CsF did not result in allyl transfer. Thus, complexes such as **2d** or **2d′** bear potential for further exploration as allyl transfer reagents.

2.1.4. Computational Analysis of the Isomerization of **2d** and **2d′**

The finding of the crystallization of **2d** by chance and the preferred crystallization of its isomer **2d′** gave rise to the question as to the relative stability of this pair of isomers and to their potentially facile interconversion in solution. With respect to THF as the solvent used for synthesis, the molecular structures of **2d** and **2d′** were optimized at the RKS PBE0 B3BJ

ZORA-def2-TZVPP level of theory with a solvent model (COSMO) of THF environment applied. A Gibbs free energy difference of 2.6 kcal·mol^{-1} in favor of the formation of allyl complex **2d′** was found (at 293 K).

In order to find a potential transition state for the interconversion of **2d** and **2d′**, two scenarios of ligand dissociation-association were considered: (a) Indicated by the molecular structure of **2d′** in the solid state (Figure 4), the two buttressing pyO ligands create an Si(μ^2-pyO)$_2$Cu eight-membered ring system, which is bridged by the allyl group. The aryl ring of the dangling pyO moiety is positioned on the same side of this ring as the allyl bridge, and thus the N atom may approach the Cu atom on the same side of the Si(μ^2-pyO)$_2$Cu eight-membered ring where the allyl group leaves. (b) Alternatively, reorientation of the dangling pyO N atom and backside attack at Cu were taken into consideration. A nudged elastic band (NEB) analysis failed to identify a transition state for scenario (a) but predicted a possible interconversion in accordance with scenario (b). This transition proceeds with initial dissociation of one ligand arm (Allyl C=C moiety or pyO N atom, depending on the direction of the conversion), followed by planarization and inversion of the Cu(N,N,Cl) coordination sphere with simultaneous bending of the Si(pyO)(Allyl) moiety to the opposite side of the eight-membered Si(μ^2-pyO)$_2$Cu ring, finalized by Cu-coordination of the respective other bridging ligand (cf. Figure S30 in the Supplementary Materials). For this scenario, a transition state with an energetic barrier of 10.6 kcal·mol^{-1} (from **2d′**) or 8.0 kcal·mol^{-1} (from **2d**) (values correspond to Gibbs free energy at 293 K) was identified (Figure 5). The energy found for this transition state already proves that the interconversion of **2d** and **2d′** should be facile at room temperature. Nonetheless, we cannot claim that this simple monomolecular scenario would be the predominant mechanism. Alternative, more complex scenarios (e.g., with Cu-ligand dissociation supported by Cu(μ^2-Cl)$_2$Cu dimerization or by coordination-dissociation effects of discrete solvent molecules) might also play reasonable roles and could potentially further lower the activation barrier.

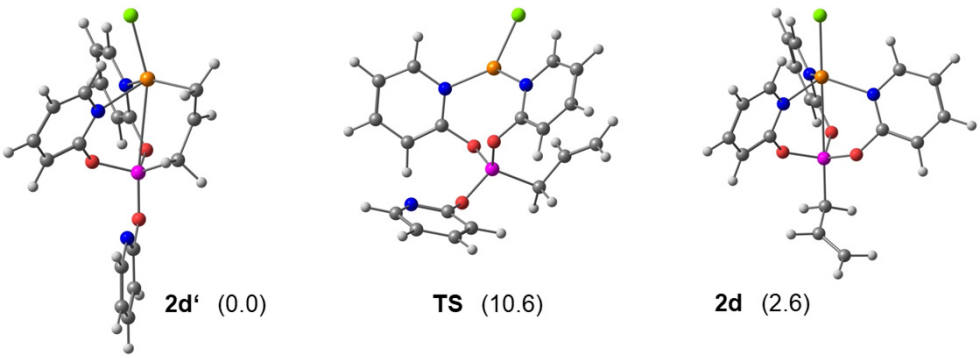

Figure 5. Optimized molecular structures of **2d′**, **2d** and the transition state (**TS**) for their interconversion with their relative Gibbs free energy (in kcal·mol^{-1}) in parentheses.

2.1.5. NMR Spectroscopic Analyses of **2b**, **2c** and **2d′**

In $CDCl_3$ solution at room temperature, compounds **2b**, **2c** and **2d′** give rise to ^{1}H and ^{13}C NMR spectra, which exhibit rather sharp signals of the nuclei of the respective different Si-bound hydrocarbyl substituents and very broad signals of the nuclei of the pyO groups (Figures 6 and 7). With respect to the latter, both the similar broadening and the similar chemical shifts of corresponding signals of the three different compounds indicate their similar conformational situation in solution. Thus, we probed whether the pyO signal broadening arises from rapid exchange (close to coalescence) of chemically different pyO ligands within one molecule or from ligand–metal dissociation/association processes (in this case, Cu–N bond dissociation and formation) within a symmetrical molecule with (on the NMR time scale) equivalent pyO ligands. For this purpose, we recorded ^{1}H (Figure 8) and ^{13}C NMR spectra (cf. Figure S16 in the the Supplementary Materials) of compound **2c** as representative examples at lower temperatures. At lower temperatures, systematic

sharpening of signals with a resultant single set of signals for the pyO moieties (four ^{1}H signals, five ^{13}C signals) was observed. We attribute the signal broadening at room temperature to predominant ligand–metal dissociation/association processes within a symmetrical molecule. This is in accordance with the molecular structures encountered within compounds **2a**, **2b**, **2c** and **2d** in the crystal structures. The relevance of allyl coordination at Cu (in case of **2d′** in solution) is particularly indicated by the noticeable upfield shift of the allyl group's olefinic ^{13}C NMR signals upon Cu complexation (**1d**: δ = 131.1 and 115.6 ppm, **2d′**: δ = 117.4 and 107.1 ppm), whereas ^{1}H NMR shifts of corresponding signals of these two compounds are similar, and even the $^{3}J_{HH}$ couplings of the -CH=CH$_2$ moiety show only little effect (**1d**: 17.1 and 10.1 Hz, **2d′**: 16.3 and 9.7 Hz for *trans*- and *cis*-$^{3}J_{HH}$ coupling, respectively).

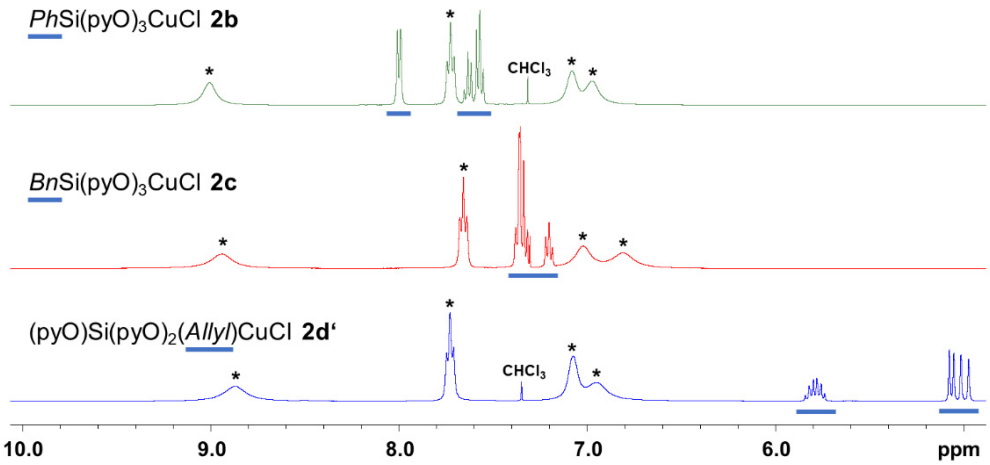

Figure 6. Aryl and olefin section of the ^{1}H NMR spectra of (from top to bottom) **2b**, **2c** and **2d′** (as solutions in CDCl$_3$, all referenced to internal SiMe$_4$ at 0 ppm, cf. Figures S9, S12 and S17 in the Supplementary Materials) recorded at 400 MHz. The asterisks (*) indicate corresponding signals of their pyO moieties, the underbars indicate the relevant ^{1}H signals of the different hydrocarbyl substituents Ph, Bn and Allyl, respectively.

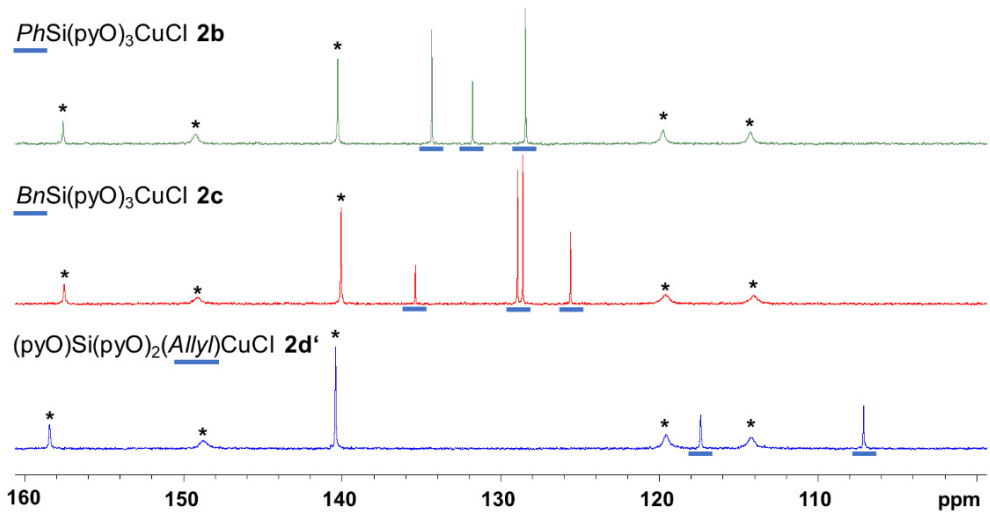

Figure 7. Aryl and olefin section of the ^{13}C NMR spectra of (from top to bottom) **2b**, **2c** and **2d′** (as solutions in CDCl$_3$, all referenced to internal SiMe$_4$ at 0 ppm, cf. Figures S10, S13 and S18 in the Supplementary Materials). The asterisks (*) indicate corresponding signals of their pyO moieties, the underbars indicate the relevant ^{13}C signals of the different hydrocarbyl substituents Ph, Bn and Allyl, respectively.

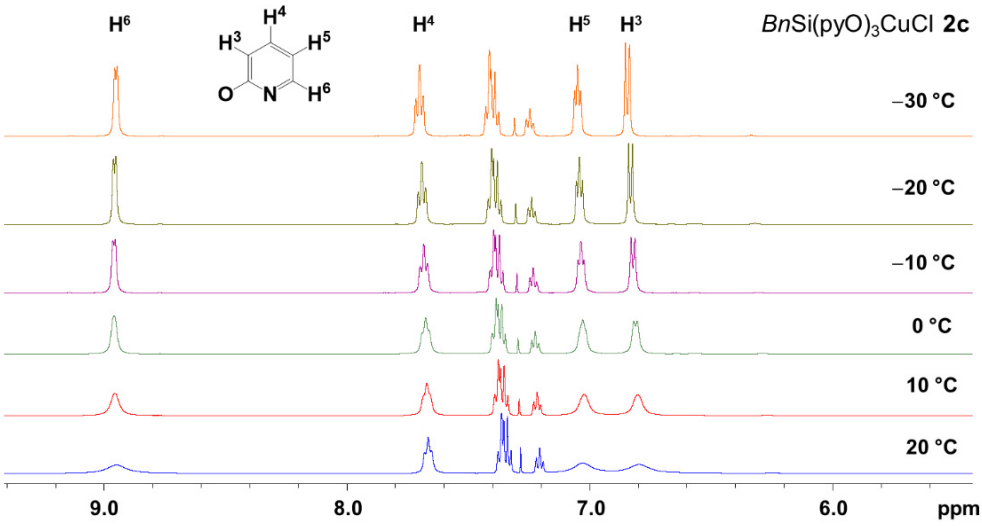

Figure 8. Aryl section of the ^{1}H NMR spectra of **2c** (as solutions in $CDCl_3$, all referenced to internal $SiMe_4$ at 0 ppm) at different temperatures, recorded at 500 MHz.

A common feature of $CDCl_3$ solutions of the herein discussed group of silanes *R*Si(pyO)$_3$ (**1a**, **1b**, **1c**, **1d**) and their corresponding Cu(I) complexes *R*Si(μ^2-pyO)$_3$CuCl is a systematic upfield shift of the ^{29}Si NMR signal upon CuCl complexation (Table 2). In cases where *R* = Me, Ph, Bn, this shift is ca. −17 ppm. For the couple with *R* = Allyl, this upfield shift is less pronounced (−12 ppm). This was unexpected, and it hints at different structural features in solutions of **2d**. In the solid state, ^{29}Si NMR spectroscopy of **2a**, **2b** and **2c** essentially confirmed the chemical shift encountered with $CDCl_3$ solutions (slightly more or less shielded Si nuclei). In case of **2d′**, however, the signal emerged close to the shift of silane **1d**. Hence, we interpret the ^{29}Si NMR shift observed with $CDCl_3$ solutions of **2d**/**2d′** as an average chemical shift which, in a dynamic equilibrium, has contributions of a propeller-type molecule **2d** (AllylSi(μ^2-pyO)$_3$CuCl coordination), causing a notable upfield shift of the signal, and contributions of its isomer **2d′** ((κO-pyO)Si(μ^2-pyO)$_2$(μ^2-Allyl)CuCl coordination), which do not cause notable upfield shift of the ^{29}Si signal with respect to silane **1d**. Thus, even though the ^{1}H and ^{13}C NMR signal broadening and shift ranges observed for pyO groups of **2d′** in $CDCl_3$ solution indicate predominance of an essentially symmetrical molecule (**2d**), the ^{29}Si shift characteristics hint at contributions of a pyO vs. allyl coordination exchange (i.e., the relevance of contributions of isomer **2d′** also in $CDCl_3$ solution).

Table 2. ^{29}Si NMR shifts (in ppm relative to $SiMe_4$) of silanes **1a** [20], **1b** [25], **1c**, **1d** and of the Cu(I) complexes thereof (**2a** [20], **2b**, **2c**, **2d′**). The shift difference between silane (**1**) and Cu(I) complex (**2**) (both in $CDCl_3$) is $\Delta\delta$ ^{29}Si (**1** vs. **2**) = δ ^{29}Si(**2**)–δ ^{29}Si(**1**). The shift difference between Cu(I) complexes (**2**) in $CDCl_3$ and in solid state is $\Delta\delta$ ^{29}Si (**2**) = δi_{so} ^{29}Si(**2**)[CP/MAS]–δ ^{29}Si(**2**) [$CDCl_3$].

R–Si =	δ ^{29}Si (*R*Si(pyO)$_3$) [$CDCl_3$] **1**	δ ^{29}Si (*R*Si(pyO)$_3$CuCl) [$CDCl_3$] **2**	$\Delta\delta$ ^{29}Si (1vs2)	δ_{iso} ^{29}Si (*R*Si(pyO)$_3$CuCl) [CP/MAS] **2**	$\Delta\delta$ ^{29}Si (2)
Me–Si **a**	−46.5 [20]	−64.1 [20]	−17.6	−70.0 [20] −71.4 [20]	−5.9 −7.3
Ph–Si **b**	−64.7 [25]	−80.9	−16.2	−82.3	−1.4
Bn–Si **c**	−54.7	−72.1	−17.4	−67.6	+4.5
Allyl–Si **d**/**d′**	−53.4	−65.4	−12.0	−52.6	+12.8

As the Cu···Si distance in compound **2d′** (3.30 Å) is similar to that in **2c** (3.23 Å), and the effect of Si hypercoordination by Cu(I) should be similar, the noticeable ^{29}Si NMR

shift differences between **2c** and **2d′** give rise to the assumption that the upfield shift encountered with CuCl complexation is only in part associated with Si hypercoordination by Cu···Si coordination. Polarization of the pyO ligands upon N···Cu coordination (and resultant changes in Si–O bonding) may play a major role. In order to probe this hypothesis, we calculated the ^{29}Si NMR shifts of compound **2b** (which was chosen because of the rather rigid hydrocarbyl substituent at Si) and a hypothetical tripodal LiCl complex of silane **1b** (PhSi(μ^2-pyO)$_3$LiCl, **2bLi**), which lacks a potential fifth lone pair donor site but still features a mono-cation to polarize the three pyO moieties (via N···Li coordination). For compound **2b**, the computational approach (COSMO model with chloroform solvent environment) predicted a ^{29}Si NMR shift of −80.8 ppm, which essentially resembles the experimental value. For the LiCl substitute **2bLi**, the same theoretical model predicted a ^{29}Si NMR shift of −75.7 ppm (which is also noticeably upfield shifted vs. −57.7 ppm for silane **1b** at the same level of theory), thus pointing at polarization via N···cation coordination as an important influence on ^{29}Si NMR shifts in complexes of silicon pyridine-2-olates.

For further solid-state characterization of these compounds, ^{63}Cu MAS NMR spectra were recorded for **2c** and **2d′** (Figure 9). From the three complexes with Cu(N,N,N,Cl) coordination sphere, compound **2c** was selected because of the only weak distortion of the Cu coordination sphere (in contrast to **2b**) and the presence of only one molecule in the crystallographic asymmetric unit (in contrast to **2a**).

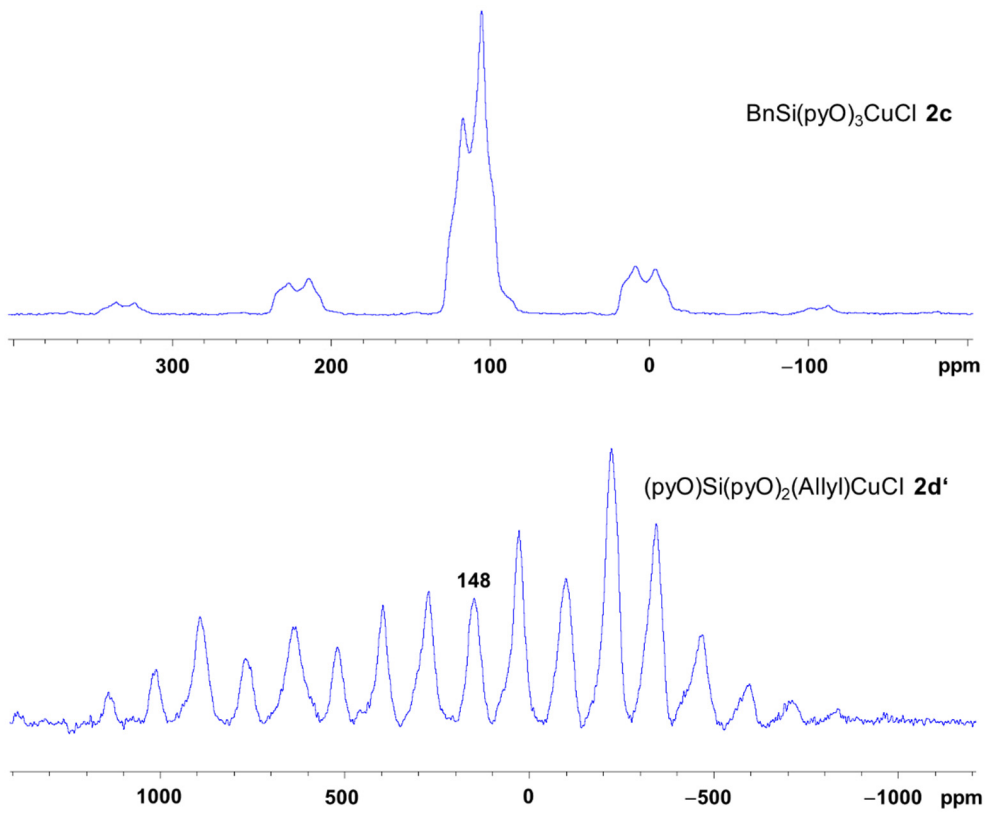

Figure 9. ^{63}Cu MAS NMR spectra of **2c** and **2d′** recorded at υ_{rot} = 20 kHz and 23 kHz, respectively. The central band in the spectrum of **2c** indicates the range of the location of δ_{iso}. In case of **2d′**, an additional spectrum was recorded at a different spinning frequency to identify the band at 148 ppm as the region in which δ_{iso} is located.

The spectra were externally referenced to CuCl, which was set at δ_{iso}(CuCl) = −332 ppm [30]. This shift is also in accordance with that of solution state experiments, in which a suspension of CuCl had been used (and set at −331 ppm) [31]. This way, the CuCl chemical shift is in agreement with the IUPAC suggested zero-point reference for ^{63}Cu solution NMR spectra (where a saturated solution of [(MeCN)$_4$Cu][ClO$_4$] in MeCN with ≤10% C$_6$D$_6$ is used as

reference) [32]. Note: In other reports, CuCl was used as zero-point reference [33,34]. In general, compounds **2c** and **2d′** produce ^{63}Cu MAS NMR spectra in which the isotropic chemical shift falls into a range of +100–+200 ppm (with CuCl set at −332 ppm). This is in accordance with Cu chemical shifts reported for other compounds close to the tetrahedral Cu coordination sphere such as $[(PhCN)_4Cu][BF_4]$ (510 ppm relative to CuCl at 0 ppm) and tetracoordinate Cu in $BrCu(PPh_3)$ (210 ppm relative to CuCl at 0 ppm) [34]. The most striking difference between the ^{63}Cu spectra of **2c** and **2d′** is the signal pattern, which is strongly influenced by the tensor of chemical shift anisotropy (CSA), quadrupolar coupling and residual dipolar coupling (the latter is caused by Cl in particular and by the N atoms to a minor extent). As expected, the compound with the more symmetric Cu coordination sphere (close to tetrahedral, **2c**) produces a rather narrow spinning side band spectrum, and the shape of the individual bands reflects the effects of quadrupolar coupling. In this case, a simulation [35] allowed for the extraction of the parameters of the chemical shift (δ_{iso} = 128 ppm) and of quadrupolar coupling (C_Q = 4.85 MHz with an asymmetry parameter η = 0.38). In spite of the mixed donor atom situation in **2c**, the quadrupolar coupling is still similar to that in the more symmetrical Cu coordination sphere of $[(PhCN)_4Cu][BF_4]$ (C_Q = 4.1 MHz [34]). In compound **2d′**, the effects of the electric field gradient (EFG) remain moderate and the signal pattern is dominated by the CSA tensor. The spinning side band spectrum resulting therefrom indicates a noticeably wider span of the CSA for compound **2d′** than for **2c**, which is in accordance with the different donor moieties in and the lower symmetry of the Cu coordination sphere of **2d′**.

*2.2. Syntheses and Crystallographic Characterization of Cu(II) Compounds RSi(μ^2-pyO)$_4$CuCl (R = Me (**3a**), Ph (**3b**), Bn (**3c**), Allyl (**3d**))*

In our previous report [20], we presented the first example of a paddlewheel complex in which Cu(II) is a potential donor atom in the coordination sphere of a hexacoordinate Si atom, compound MeSi(μ^2-pyO)$_4$CuCl (**3a**). The Cu···Si distance (2.919(1) Å) indicated attraction of the two atoms, and a natural localized molecular orbital (NLMO) analysis indicated some polarization of one of the Cu atom's d-orbitals toward Si. As in this initial study compound **3a** was obtained only in small amounts as a decomposition product of Cu(I) complex **2a**, we now aimed to establish a deliberate synthesis route of this class of compounds and to prepare some analogs of this series for comparison of their molecular structures with regard to the response of the Cu(II)–Si-interaction to the different *trans*-disposed hydrocarbyl substituents. Starting from silanes *R*Si(pyO)$_3$ (**1a**–**d**) and CuCl, the oxygen content of dry air (in a close to stoichiometric manner) was used as an oxidant, and excess silane needed to be employed as a source of additional pyO ligands and a scavenger of oxide formed in the redox reaction. Scheme 2 gives an impression of the targeted reaction. (Note: For the by-products of oxide capture, siloxanes, only a symbolic example is drawn. The portfolio of siloxanes formed has not been characterized.) For that purpose, the respective amounts of silane **1** and CuCl (in approximate stoichiometric ratio 3:2) were placed in a Schlenk flask under a dry argon atmosphere and dissolved into a small amount of THF, whereafter the calculated amount of air (which had been stored in a flask over anhydrous $CaCl_2$ for at least one week) was added to the gas phase in the Schlenk flask via syringe. Syntheses of **3a**, **3b** and **3c** were successful. Within a few days, dark blue crystals of the desired product formed in good yield. In case of conversion of **1d** and CuCl, however, a brown precipitate formed in the blue solution. The crystals of **3b** and **3c** were of good quality for X-ray diffraction analysis (Figure 10, Table A3). Some crystals of **3d** (not in a deliberate manner to determine yield and purity, but of sufficient quality for single-crystal X-ray diffraction analysis) were obtained along the initial "by chance" method, i.e., allowing access of traces of air to one of the synthesis batches of **2d**, where silane **1d** and CuCl were used in an approximately 1:1 stoichiometric ratio. For comparison of the molecular structures, selected atom distances and angles are listed in Table 3.

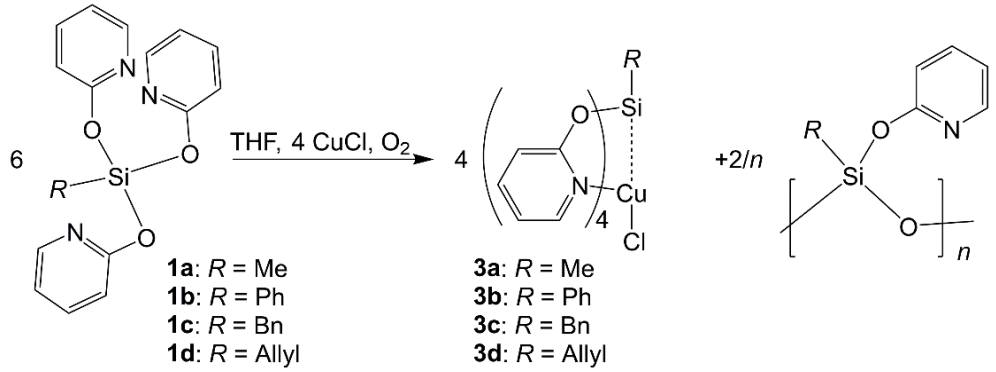

Scheme 2. Generic scheme of the syntheses of Cu(II) complexes (**3a**, **3b**, **3c**, **3d**) from silanes *R*Si(pyO)$_3$, (**1a**, **1b**, **1c**, **1d**, respectively) and dry air.

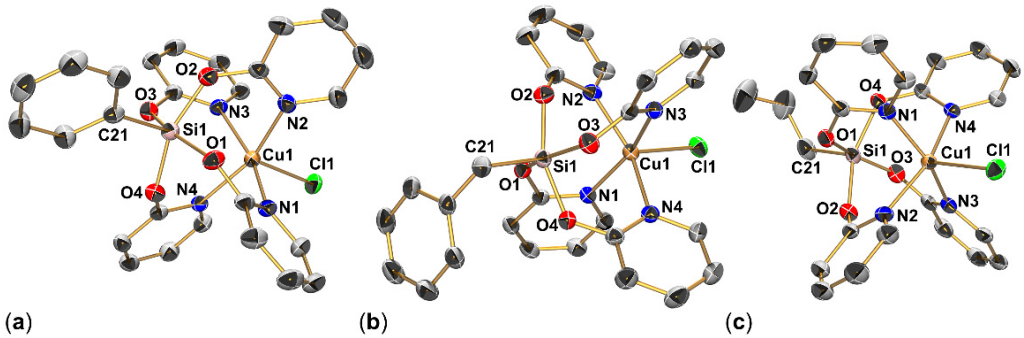

Figure 10. Molecular structures of (**a**) **3b**, (**b**) **3c** and (**c**) **3d** with thermal displacement ellipsoids at the 50% probability level and labels of selected non-hydrogen atoms. Hydrogen atoms are omitted for clarity. Selected interatomic distances and angles are listed in Table 3.

Table 3. Selected atom distances (Å) and bond angles (deg) in compounds **3b**, **3c** and **3d** in their crystal structures (as well as some corresponding parameters of **3a** [20]).

	3a	3b	3c	3d
Si1–O1	1.753(2)	1.765(2)	1.744(2)	1.742(2)
Si1–O2	1.757(2)	1.733(2)	1.750(2)	1.757(2)
Si1–O3	1.753(2)	1.764(2)	1.756(2)	1.752(2)
Si1–O4	1.755(2)	1.746(2)	1.746(2)	1.746(2)
Si1–C21	1.847(2)	1.861(2)	1.870(2)	1.857(3)
Cu1–N1	2.023(2)	2.047(2)	2.042(2)	2.028(2)
Cu1–N2	2.055(2)	2.029(2)	2.057(2)	2.035(2)
Cu1–N3	2.025(2)	2.038(2)	2.055(2)	2.052(2)
Cu1–N4	2.049(2)	2.034(2)	2.044(2)	2.019(2)
Cu1–Cl1	2.403(1)	2.389(1)	2.403(1)	2.395(1)
Cu1···Si1	2.919(1)	2.888(1)	2.915(1)	2.897(1)
O1–Si1–O3	154.22(6)	157.60(8)	154.98(8)	155.82(9)
O2–Si1–O4	155.83(6)	154.21(8)	154.14(8)	153.49(9)
N1–Cu1–N3	159.32(5)	159.23(8)	158.15(7)	157.76(9)
N2–Cu1–N4	158.66(5)	160.00(8)	159.05(7)	159.26(9)
Cl1–Cu1···Si1	178.24(2)	177.27(2)	179.43(2)	178.15(3)
Cu1···Si1–C21	177.51(6)	177.99(8)	176.47(8)	177.16(11)

The four paddlewheel shaped compounds of type **3** exhibit essentially the same cage structure, in which Si and Cu atom are situated in square-based pyramidal coordination spheres with basal (O)$_4$ and (N)$_4$ coordination, respectively, and axial monodentate substituents (hydrocarbyl and Cl, respectively). The sets of Si–O and Cu–N bond lengths do not exhibit any systematic trends of deviations, and Cu···Si distances only vary in a narrow

range (2.89–2.92 Å). In contrast to complexes of type **2**, the variation of Cu···Si distances in compounds **3** hints at systematic response of this interatomic interaction to the different Si-bound hydrocarbyl substituents, as the Si-Ph derivative **3b** features the shortest Cu···Si contact, the Si-Me compound **3a** the longest.

The crystal structure of compound **3b** is reminiscent of the structures of the paddlewheel complexes PhSb(μ^2-pyO)$_4$Ru(CO) and PhSb(μ^2-pyO)$_4$RuCl [36], which crystallize in the same orthorhombic space group *Pbca* with isomorphous unit cell parameters. In the former case, some essential molecular metrics adhere to the same proportions (distance between opposite pyO-C^4 atoms in the paddlewheel 9.42 and 9.46 Å, distance between Cl atom and Ph-p-C atom 9.94 Å for **3b**; distance between opposite pyO-C^4 atoms in the paddlewheel 9.86 and 9.87 Å, distance between carbonyl O atom and Ph-p-C atom 10.41 Å for PhSb(μ^2-pyO)$_4$Ru(CO)). In the latter case, the distance between Cl atom and Ph-p-C atom (9.86 Å) is similar to that in **3b**, whereas the distances between opposite pyO-C^4 atoms in the paddlewheel (9.81 and 9.82 Å) are similar to those in PhSb(μ^2-pyO)$_4$Ru(CO).

2.3. Reaction of $Ph_2Si(pyO)_2$ and CuCl

For a comparison of CuCl complexation with a pyO functionalized silane of the type R_2Si(pyO)$_2$, the diphenyl derivative Ph$_2$Si(pyO)$_2$ (**4**) [26] was chosen as its aryl groups may support crystallization (and thus support solid-state characterization of the products). Furthermore, the phenyl ring still offers an alternative ligand motif through coordination of its π-electron system to Cu(I) (if required). Benzene rings have already proven capable of coordinating Cu(I). Even in rather simple compounds obtained from CuCl and ZrCl$_4$, benzene itself may serve as a ligand in the Cu(I) coordination sphere [37,38].

Reaction of **4** and CuCl in THF proceeded instantly with dissolution of CuCl. Within a few hours, crystallization commenced and produced a mixture of yellow and colorless crystals of sufficient quality for single-crystal X-ray diffraction analysis. The former were identified as compound [Ph$_2$Si(μ^2-pyO)$_2$(CuCl)$_2$(μ^2-pyO)$_2$SiPh$_2$] (**5^2**), which adheres to the stoichiometry of **4** and CuCl used (Scheme 3, Table A4, Figure 11). The latter were identified as THF solvate of compound [Ph$_2$Si(μ^2-pyO)$_2$(CuCl)$_4$(μ^2-pyO)$_2$SiPh$_2$] (**5^4**), which features excessive CuCl in its molecular structure in a distorted ladder-type motif (Table A4, Figure 12). Repeated reaction of **4** and CuCl (even with use of excess of silane **4**) failed to produce **5^2** but delivered the THF solvate of **5^4** as the exclusive solid product in good yield. This observation hints at the co-existence of various species (such as **4**, **5^2** and **5^4**) in solution in equilibrium and solvent-driven crystallization of **5^4**. Therefore, the synthesis was repeated in chloroform as an alternative solvent. In spite of the slight excess of **4** used, another CuCl-excess complex crystallized. In this case, a CHCl$_3$ solvate of compound [Ph$_2$Si(μ^2-pyO)$_2$(CuCl)$_3$(μ^2-pyO)$_2$SiPh$_2$] (**5^3**) crystallized, which also features the excessive CuCl in its molecular structure in a ladder-type arrangement (Table A4, Figure 11).

In the molecules of **5^2**, **5^3** and **5^4** the Cu···Si atom distances range between 3.52 and 3.64 Å. These distances are noticeably longer than those in Cu(I) compounds **2a**–**2d** (ca. 3.2 Å) or compound **2d′** (3.3 Å). The Si atom merely plays a role as a backbone building block, which connects the two Cu-coordinating pyO moieties. The Si-bound phenyl groups remain at the periphery of the molecules and do not establish coordination with the Cu atoms. A common feature of the Si coordination spheres of **5^2**, **5^3** and **5^4** is the widening of the O–Si–O angles (both the C–Si–C and O–Si–O angles are wider than the tetrahedral angle). With respect to the central (CuCl)$_n$ parts, only the well-ordered structures of **5^2** and **5^3** will be taken into consideration for discussion. The pyO-chelated Cu atoms are located in highly distorted tetrahedral coordination spheres, which feature wide N–Cu–N angles (ranging from 123° to 136°) and Cl–Cu–Cl angles in the range of 95–100°. The former can be interpreted as a result of the small bond angles within the four-membered Cu$_2$Cl$_2$-rings. In the three compounds case, bridging Cu–Cl–Cu-coordination is the favored motif to accomplish tetracoordination of the (pyO)$_2$-chelated Cu atoms, and in **5^3** and **5^4**, the central Cu sites in the (CuCl)$_n$ ladder motifs remain tricoordinate. The resultant Cu$_2$Cl$_2$-rings can be planar (as in the case of **5^2**, resulting from a crystallographically imposed center of

inversion) and may also deviate noticeably from planarity as one of the two Cu_2Cl_2-rings in **5³**. In the latter compound, Cu1, Cl1, Cu2 and Cl2 are still close to planarity (the angle between the planes Cu1Cl1Cu2 and Cu1Cl2Cu2 is 8.02(7)°), whereas the angle between the planes Cu2Cl2Cu3 and Cu2Cl3Cu3 is 40.27(5)°. Even in the planar Cu_2Cl_2 ring in **5²**, this ring is of rather low symmetry as it features asymmetric Cu–Cl–Cu bridges (CuCl bond lengths of 2.301(1) and 2.624(1) Å). In contrast, in the less symmetric molecule **5³**, the Cu_2Cl_2 rings may exhibit symmetric (Cu1–Cl2 2.533(2), Cu2–Cl2 2.527(2) Å) and less symmetric Cu–Cl–Cu bridges (Cu1–Cl1 2.450(2), Cu2–Cl1 2.158(2) Å). These selected examples already indicate very high flexibility of $(CuCl)_n$ cores in their multinuclear complexes, and ladder-type complexes thereof with terminal Cu-complexation by chelating ligands are just one among other motifs: The portfolio of literature-known complexes with $(CuCl)_n$ cores offers examples for further motifs (Figure 13), e.g., with n = 1 and 2 within one molecule (**XVI** [39]), n = 3 ladder-type with ligands bridging Cu-positions 1 and 3 (**XVII** [40]) or with monodentate ligands at Cu in positions 1 and 3 (**XVIII** [41]), n = 3 cyclic motif with two Cu atoms chelated (**XIX** [42]) or three Cu atoms chelated (**XX** [43]) and $(CuCl)_4$-cubes with additional ligands at Cu (e.g., **XXI** and **XXII**, which feature N-donor ligands [44]). Ligands capable of monodentate bridging (such as thiourea derivatives), which adopt the bridging role of the Cl atom, enhance the portfolio of complexes with $(CuCl)_n$ cores even further, e.g., in compound **XXIII** [45].

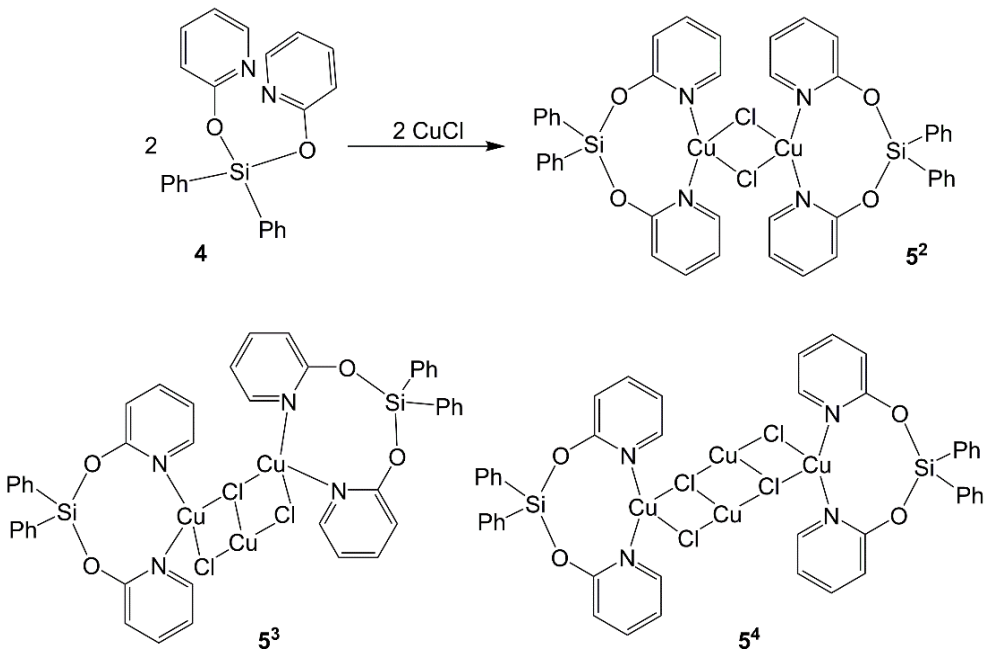

Scheme 3. Reaction of silane $Ph_2Si(pyO)_2$ (**4**) and CuCl with formation of compound **5²** and sketches of products **5³** and **5⁴** obtained from this reaction.

The variety of coordination motifs accessible for CuCl-oligomers is manifold, and lowering the number of donor arms in a ligating system (e.g., going from silane **2b** to **4** by replacing one pyO unit by Ph) opens coordination sites at Cu for CuCl-coordination. The selection of compounds **5ⁿ** (n = 2, 3, 4), which were obtained from 1:1 stoichiometric reactions of **4** and CuCl, hints at a greater variety of species in the reaction solutions and solubility driven crystallization of the one or the other species. This hampered characterization in solution. The two compounds (**5³** and **5⁴**), which were isolated as pure products, decomposed upon dissolution in $CDCl_3$. In both cases, a yellow solution and a beige precipitate formed, and both solutions produced essentially identical ^1H, ^{13}C and ^{29}Si NMR spectra. In the ^{29}Si spectrum, a single signal at −43.9 ppm indicates the formation of a new tetracoordinate Si-compound rather than the release of ligand **4**. Silane **4** in $CDCl_3$ produces a signal at −33.1 ppm [26]. In addition, the solids **5³**·($CHCl_3$) (δ_{iso} = −32.9, −33.5 ppm)

and $\mathbf{5^4}\cdot(THF)_2$ (δ_{iso} = −32.4 ppm) produce ^{29}Si NMR signals close to the ^{29}Si chemical shift of compound **4**. The broad signals of the pyO moieties in the ^{1}H and ^{13}C spectra hint at rapid exchange processes. The flexibility of these ligand systems (of compound **4**, and most likely the same is true for related silanes) poses challenges for the deliberate synthesis of simple complexes of a desired stoichiometry and for the characterization of their CuCl complexes in solution.

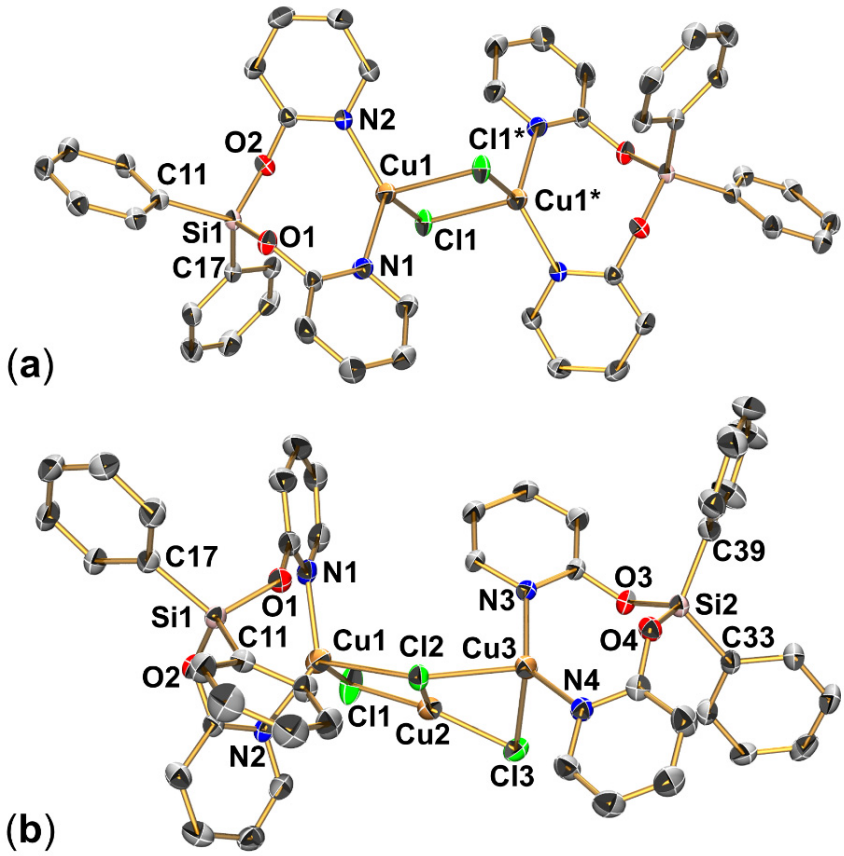

Figure 11. Molecular structures of (**a**) $\mathbf{5^2}$ and (**b**) $\mathbf{5^3}$ in its chloroform solvate $\mathbf{5^3}\cdot(CHCl_3)$ with thermal displacement ellipsoids at the 50% probability level and labels of selected non-hydrogen atoms. Hydrogen atoms are omitted for clarity. Selected interatomic distances (Å) and angles (deg) for $\mathbf{5^2}$: Cu1–Cl1 2.301(1), Cu1–Cl1* 2.624(1), Cu1–N1 2.059(2), Cu1–N2 1.996(2), Si1–O1 1.644(2), Si1–O2 1.648(2), Cl1–Cu1–Cl1* 100.33(2), Cu1–Cl1–Cu1* 79.67(2), N1–Cu1–N2 122.71(6), O1–Si1–O2 111.90(7), C11–Si1–C17 114.45(8); $\mathbf{5^3}$: Cu1–Cl1 2.4499(13), Cu1–Cl2 2.5331(11), Cu2–Cl1 2.1578(13), Cu2–Cl2 2.5274(13), Cu2–Cl3 2.1685(12), Cu3–Cl2 2.5043(11), Cu3–Cl3 2.5512(12), Cu1–N1 1.990(4), Cu1–N2 2.000(4), Cu3–N3 1.986(3), Cu3–N4 1.994(3), Si1–O1 1.646(3), Si1–O2 1.650(3), Si2–O3 1.649(3), Si2–O4 1.648(3), Cl1–Cu1–Cl2 99.50(4), Cl2–Cu3–Cl3 94.96(4), N1–Cu1–N2 131.81(14), N3–Cu3–N4 136.28(14), O1–Si1–O2 109.99(15), C11–Si1–C17 116.62(19), O3–Si2–O4 109.94(15), C33–Si2–C39 118.73(19).

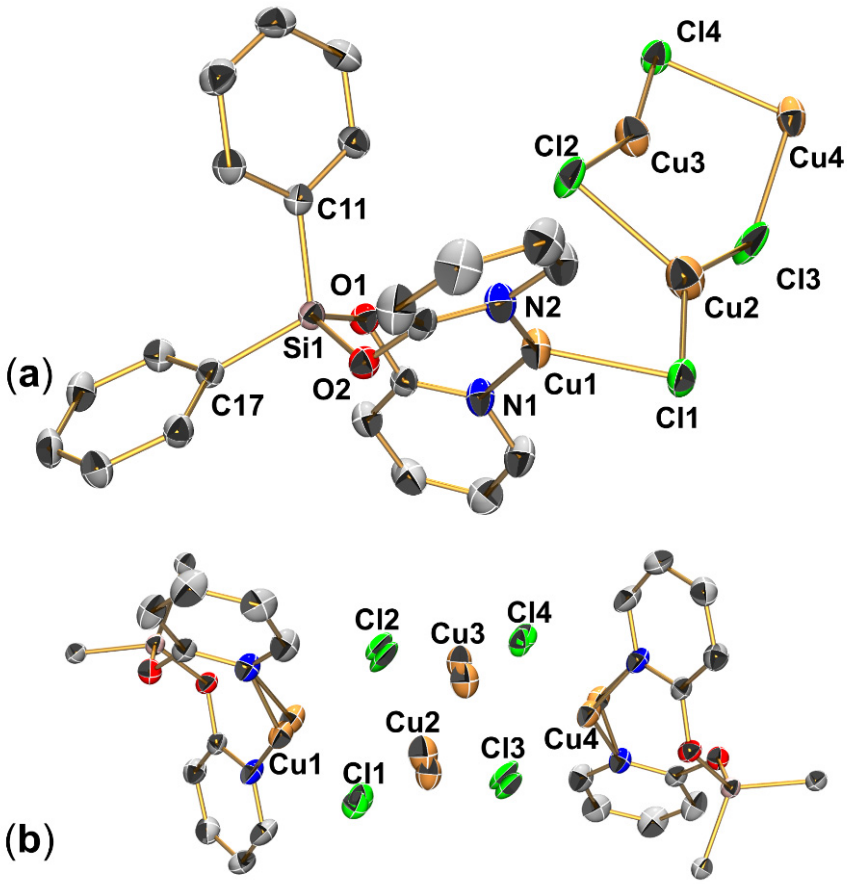

Figure 12. Molecular structure of **5⁴** in its THF solvate **5⁴**·$(THF)_2$ with thermal displacement ellipsoids at the 50% probability level and labels of selected non-hydrogen atoms. Section (**a**) shows the asymmetric unit, section (**b**) shows the central part of the molecule with positions of the Cu and Cl atoms, which result from disorder by symmetry. For each group of two Cu or Cl atoms, the atom labels are located next to the atom which is part of the asymmetric unit. (The molecule is located on a center of inversion. Only the periphery, the two $Ph_2Si(pyO)_2$ motifs, adhere to this symmetry, whereas the central Cu_4Cl_4 part appears disordered and its Cu and Cl atoms can be refined in two positions. As there had been no superstructure reflections in the data set, which would hint at a larger unit cell, and refinement in space group *P*1 did not eliminate this disorder, a selected set of the Cu and Cl atoms was chosen as a possible actual asymmetric unit.) Selected interatomic distances (Å) and angles (deg) for **5⁴**: Si1–O1 1.649(2), Si1–O2 1.650(2), O1–Si1–O2 111.92(7), C11–Si1–C17 113.58(8).

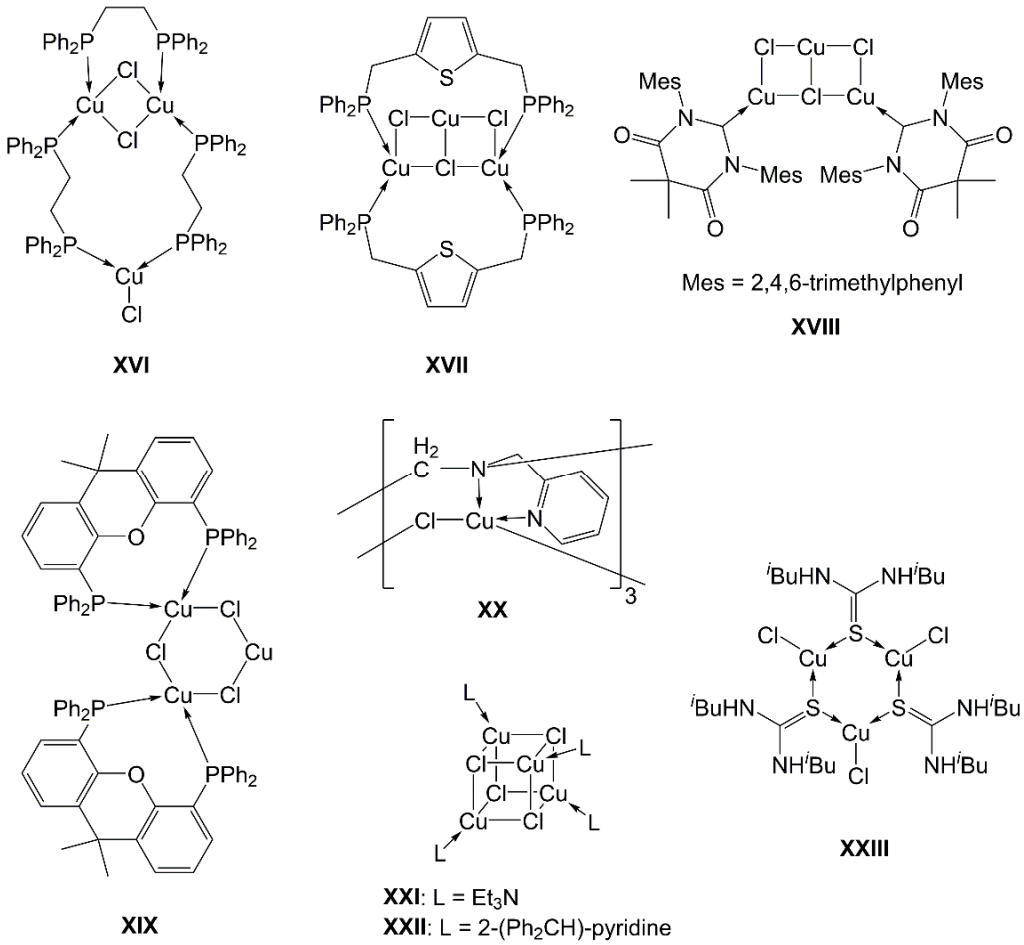

Figure 13. Selected examples of oligonuclear complexes with $(CuCl)_n$ cores (n = 1, 2, 3, 4; **XVI**–**XXII**) as well as an example of a complex with bridged (CuCl)-motifs (**XXIII**). For reasons of clarity of presentation, formal lone pair donation by L-type ligands (such as phosphanes) is indicated by a dative bond arrow, whereas X-type bonds (for example CuCl, even in case of bridging bonds of mixed L,X-type) are indicated by a regular bond dash.

3. Materials and Methods

3.1. General Considerations

Starting materials 2-hydroxypyridine (ABCR, Karlsruhe, Germany, 98%), benzyltrichlorosilane (ABCR, Karlsruhe, Germany, 98%) and allyltrichlorosilane were used as received without further purification. Silanes $MeSi(pyO)_3$ (**1a**) [20], $PhSi(pyO)_3$ (**1b**) [25] and $Ph_2Si(pyO)_2$ (**4**) [26] as well as CuCl [46] have been available from our previous studies. THF, diethyl ether and triethylamine were distilled from sodium/benzophenone and kept under argon atmosphere. *n*-Pentane (Th.Geyer, Renningen, Germany, >99%), chloroform, stabilized with amylenes (Honeywell, Seelze, Germany, ≥99.5%) and $CDCl_3$ (Deutero, Kastellaun, Germany, 99.8%) were stored over activated molecular sieves (3 Å) for at least 7 days and used without further purification. All reactions were carried out under an atmosphere of dry argon utilizing standard Schlenk techniques. (The silanes and Cu complexes reported in this paper are sensitive toward hydrolysis, and the Cu(I) complexes are sensitive toward oxidation.) Solution NMR spectra (^1H, ^{13}C, ^{29}Si) (cf. Figures S3–S23 in the Supplementary Materials) were recorded on Bruker Avance III 500 MHz and Bruker Nanobay 400 MHz spectrometers. ^1H, ^{13}C and ^{29}Si chemical shifts are reported relative to Me_4Si (0 ppm) as the internal reference. ^1H and ^{13}C NMR signals were assigned in accordance with mutual coupling patterns (in case of ^1H) and according to the shifts of corresponding ^1H or ^{13}C NMR signals in related compounds $MeSi(pyO)_3$ [20], $Ph_2Si(pyO)_2$ [26] and $PhP(pyO)_2$ [47]. Furthermore, ^1H-^{13}C-HSQC NMR spectra of compounds **1c** and **2c**

were recorded to confirm signal assignments of corresponding pyO ^{13}C signals within groups of compounds *R*Si(pyO)$_3$ and *R*Si(μ^2-pyO)$_3$CuCl, respectively. ^{29}Si CP/MAS NMR spectra (cf. Figures S24–S29 in the Supplementary Materials) were recorded on a Bruker Avance 400 WB spectrometer using 4 mm zirconia (ZrO_2) rotors and an MAS frequency of υ_{rot} = 5 kHz. The chemical shift is reported relative to Me_4Si (0 ppm) and was referenced externally to octakistrimethylsiloxyoctasilsesquioxane Q_8M_8 (the most upfield signal of its Q^4 groups at δ_{iso} = −109 ppm). ^{63}Cu MAS NMR spectra were recorded on a Bruker Avance Neo 700 SB spectrometer using 3.2 mm zirconia (ZrO_2) rotors and MAS frequencies of up to υ_{rot} = 23 kHz. The chemical shift is reported relative to and referenced with a sample of CuCl (at δ_{iso} = −332 ppm). Elemental analyses were performed on an Elementar Vario MICRO cube. For single-crystal X-ray diffraction analyses, crystals were selected under an inert oil and mounted on a glass capillary (which was coated with silicone grease). Diffraction data were collected on a Stoe IPDS-2/2T diffractometer (STOE, Darmstadt, Germany) using Mo Kα-radiation. Data integration and absorption correction were performed with the STOE softwares XArea and XShape, respectively. The structures were solved by direct methods using SHELXS-97 or SHELXT and refined with the full-matrix least-squares methods of F^2 against all reflections with SHELXL-2014/7 or SHELXL-2018/3 [48–52]. All non-hydrogen atoms were anisotropically refined, and hydrogen atoms were isotropically refined in idealized position (riding model). For details of data collection and refinement (incl. the use of SQUEEZE in the refinement of the structure of **5^4**), see Appendix A, Tables A1–A4. Graphics of molecular structures were generated with ORTEP-3 [53,54] and POV-Ray 3.7 [55]. CCDC 2,222,519 (**5^2**), 2,222,520 (**1d**), 2,222,521 (**2c**), 2,222,522 (**3b**), 2,222,523 ((**5^4**)·(THF)$_2$), 2,222,524 (**3c**), 2,222,525 (**1c**), 2,222,526 (**3d**), 2,222,527 (**2d′**), 2,222,528(**2d**), 2,222,529 ((**2b**)$_2$·(THF)), and 2,222,530 ((**5^3**)·($CHCl_3$)), contain the supplementary crystal data for this article. These data can be obtained free of charge from the Cambridge Crystallographic Data Centre via https://www.ccdc.cam.ac.uk/structures/ (accessed on 27 November 2022).

All geometry optimizations and NEB (Nudged Elastic Band Method) calculations were carried out with ORCA 5.0.3 [56] using the restricted PBE0 functional with relativistically recontracted Karlsruhe basis sets ZORA-def2-TZVPP [57,58] (for all atoms), the scalar relativistic ZORA Hamiltonian [59,60], atom-pairwise dispersion correction with the Becke–Johnson damping scheme (D3BJ) [61,62] and COSMO solvation (THF: ε = 7.58, rsolv = 3.18; $CHCl_3$: ε = 4.8, rsolv = 3.17). VeryTightSCF and slowconv options were applied and the DEFGRID3 was used with a radial integration accuracy of 10 for copper and silicon for all calculations. Calculations were started from the molecular structures obtained by single-crystal X-ray diffraction analysis and isomers were created by modifying these structures. Numerical frequency calculations were performed to prove convergence at the local minimum after geometry optimization and to obtain the Gibbs free energy (293.15 K). On the final structures, single-point calculations were performed with a restricted B2T-PLYP functional with relativistically recontracted Karlsruhe basis sets ZORA-def2-TZVPP [57,58] (for all atoms) and by utilizing the AutoAux generation procedure [63], relaxed MP2 densities, the scalar relativistic ZORA Hamiltonian [59,60], atom-pairwise dispersion correction with the Becke–Johnson damping scheme (D3BJ) [61,62] and COSMO solvation (THF). The transition state search was started from the geometry of step five of the NEB calculation and confirmed with numerical frequency calculations. NMR calculations were performed using ORCA 5.0.3 [56] with GIAO formalism using the restricted PBE0 functional with relativistically recontracted Karlsruhe basis sets ZORA-def2-TZVPP [57,58] (for all atoms), the scalar relativistic ZORA Hamiltonian [59,60], atom-pairwise dispersion correction with the Becke–Johnson damping scheme (D3BJ) [61,62] and COSMO solvation ($CHCl_3$: ε = 4.8, rsolv = 3.17). NMR chemical shifts were referenced against tetramethylsilane. Graphics of the optimized molecular structures were generated using Chemcraft [64].

3.2. Syntheses and Characterization

Compound **2b** (PhSi(μ^2-pyO)$_3$CuCl)$_2$·(THF) ($C_{46}H_{42}Cl_2Cu_2N_6O_7Si_2$). Under dry argon atmosphere, a Schlenk flask was charged with magnetic stirring bar, silane **1b** (PhSi(pyO)$_3$·0.5(THF), 1.025 g, 2.23 mmol) and CuCl (0.195 g, 1.97 mmol), whereafter THF (3 mL) was added. The resultant mixture was stirred in a water bath (40 °C) for few minutes to afford a clear light yellow (slightly greenish-yellow) solution. Upon cooling to room temperature, this Schlenk flask was connected to another flask with *n*-pentane (5 mL) for gas phase diffusion of pentane into the solution. The product crystallized within 1 d, whereupon the supernatant was decanted, and the solid product was washed with a mixture of THF (2 mL) and *n*-pentane (1 mL) and briefly dried in vacuum. Yield: 0.97 g (0.928 mmol, 94%) of (**2b**)$_2$·(THF). Elemental analysis indicated loss of some solvent upon sample preparation. Calculated for $C_{21}H_{17}ClCuN_3O_3Si$·0.3(THF) (508.09 g·mol^{-1}): C, 52.48%; H, 3.85%; N, 8.27%; found C, 52.5%; H, 3.9%; N, 8.3%. ^{1}H NMR ($CDCl_3$): δ (ppm) 9.01 (br, 3H, H^6), 8.00 (m, 2H, Ph-o), 7.72 (m, br, 3H, H^4), 7.66–7.60 (m, 1H, Ph-p), 7.60–7.54 (m, 2H, Ph-m), 7.08 (br, 3H, H^5), 6.97 (br, 3H, H^3); ^{13}C{^{1}H} NMR ($CDCl_3$): δ (ppm) 157.6 (C^2), 149.2 (C^6), 140.3 (C^4), 134.3 (Ph-o), 131.8 (Ph-p), 128.4 (Ph-m), 128.4 (Ph-i), 119.8 (C^5), 114.2 (C^3); ^{29}Si{^{1}H} NMR ($CDCl_3$): δ (ppm) −80.9; (CP/MAS): δ_{iso} (ppm) −82.3.

Compound **2c** BnSi(μ^2-pyO)$_3$CuCl ($C_{22}H_{19}ClCuN_3O_3Si$). Under dry argon atmosphere, a Schlenk flask was charged with magnetic stirring bar, silane **1c** (0.49 g, 1.22 mmol) and CuCl (0.115 g, 1.16 mmol), whereafter THF (1.5 mL) was added. The resultant mixture was briefly stirred at room temperature until complete dissolution of CuCl was achieved (some crystals of **1c** still remained undissolved) to afford a light yellow (slightly greenish-yellow) solution, which was then stored undisturbed at room temperature. Crystallization of **2c** commenced within some minutes, and the initially undissolved silane **1c** dissolved during crystallization of **2c**. After 4 d, the supernatant was decanted, and the coarse crystalline yellow product was dried in vacuum. Yield: 0.50 g (1.00 mmol, 86%) of **2c**. Elemental analysis calculated for $C_{22}H_{19}ClCuN_3O_3Si$ (500.49 g·mol^{-1}): C, 52.80%; H, 3.83%; N, 8.40%; found C, 52.6%; H, 4.0%; N, 8.4%. ^{1}H NMR ($CDCl_3$): δ (ppm) 8.94 (br, 3H, H^6), 7.66 (m, br, 3H, H^4), 7.40–7.29 (mm, 4H, Ph-o/m), 7.24–7.17 (m, 1H, Ph-p), 7.02 (br, 3H, H^5), 6.81 (br, 3H, H^3), 2.76 (s, 2H, CH$_2$); ^{13}C{^{1}H} NMR ($CDCl_3$): δ (ppm) 157.5 (C^2), 149.1 (C^6), 140.1 (C^4), 135.4 (Ph-i), 128.9, 128.6 (Ph-o/m), 125.6 (Ph-p), 119.6 (C^5), 114.0 (C^3), 22.2 (CH$_2$); ^{29}Si{^{1}H} NMR ($CDCl_3$): δ (ppm) −72.1; (CP/MAS): δ_{iso} (ppm) −67.6.

Compounds **2d/2d′** AllylSi(μ^2-pyO)$_3$CuCl/(κO-pyO)Si(μ^2-pyO)$_2$(μ^2-Allyl)CuCl ($C_{18}H_{17}ClCuN_3O_3Si$). Under a dry argon atmosphere, a Schlenk flask was charged with a magnetic stirring bar, silane **1d** (0.45 g, 1.28 mmol) and CuCl (0.114 g, 1.15 mmol), whereafter THF (3 mL) was added. The resultant mixture was briefly stirred at room temperature until complete dissolution of CuCl was achieved to afford a light yellow (slightly greenish-yellow) solution, which was passed through a syringe filter to remove some turbidity before *n*-pentane (6 mL) was added. From this mixture, the product separated as a yellow oil. Storage at 5 °C and then at room temperature afforded crystalline **2d′** as a colorless solid, which was isolated from the supernatant by decantation, washed with a mixture of THF (1 mL) and *n*-pentane (2 mL) and dried in vacuum. Yield: 0.43 g (0.95 mmol, 83%) of **2d′**. Elemental analysis calculated for $C_{18}H_{17}ClCuN_3O_3Si$ (450.42 g·mol^{-1}): C, 48.00%; H, 3.80%; N, 9.33%; found C, 47.89%; H, 4.32%; N, 9.33%. (In a similar synthesis, the yellow oil solidified with formation of crystals of **2d**, which were suitable for single-crystal X-ray diffraction analysis, but then re-crystallized in the mother liquor with formation of **2d′** before **2d** had been isolated as a pure solid.) ^{1}H NMR ($CDCl_3$): δ (ppm) 8.87 (br, 3H, H^6), 7.73 (m, br, 3H, H^4), 7.08 (br, 3H, H^5), 6.95 (br, 3H, H^3), 5,79 (m, 1H, =CH), 5.06 (m, 1H, incl. $^3J_{HH(cis)}$ 9.7 Hz, =CH$_2$), 4.99 (m, 1H, incl. $^3J_{HH(trans)}$ 16.3 Hz, =CH$_2$), 2.21 (d, 2H, 7.6 Hz, CH$_2$); ^{13}C{^{1}H} NMR ($CDCl_3$): δ (ppm) 158.4 (C^2), 148.7 (C^6), 140.4 (C^4), 119.6 (C^5), 117.4 (Allyl =CH), 114.2 (C^3), 107.1 (Allyl =CH$_2$), 20.5 (CH$_2$); ^{29}Si{^{1}H} NMR ($CDCl_3$): δ (ppm) −65.4; (CP/MAS): δ_{iso} **2d′** (ppm) −52.6.

Compound **3a** MeSi(μ^2-pyO)$_4$CuCl ($C_{21}H_{19}ClCuN_4O_4Si$). Under a dry argon atmosphere, a Schlenk flask (volume ca. 50 mL) was charged with magnetic stirring bar, silane

1a ($MeSi(pyO)_3$, 229 mg, 0.70 mmol) and CuCl (46 mg, 0.46 mmol), whereafter THF (2 mL) was added. The resultant mixture was stirred in a water bath (45 °C) for few minutes to afford a clear light yellow (slightly greenish-yellow) solution. Upon cooling to room temperature, dry air (12 mL, corresponding to ca. 0.105 mmol of O_2) was added into the lower half of gas phase of this Schlenk flask via syringe through a septum, and excess argon was allowed to leave through an oil trap before the flask was closed. Within minutes, the color of the solution turned deep blue, and formation of dark blue crystals commenced within a few hours. The contents were stored undisturbed at room temperature overnight, whereupon the supernatant was decanted, and the solid product was washed with THF (0.5 mL) and dried in vacuum. Yield: 156 mg (0.30 mmol, 73%) of **3a**. Elemental analysis calculated for $C_{21}H_{19}ClCuN_4O_4Si$ (518.48 g·mol^{-1}): C, 48.65%; H, 3.69%; N, 10.81%; found C, 48.80%; H, 4.02%; N, 10.55%.

Compound **3b** $PhSi(\mu^2\text{-pyO})_4CuCl$ ($C_{26}H_{21}ClCuN_4O_4Si$). Under a dry argon atmosphere, a Schlenk flask (volume ca. 50 mL) was charged with magnetic stirring bar, silane **1b** ($PhSi(pyO)_3$·0.5(THF), 288 mg, 0.63 mmol) and CuCl (42 mg, 0.42 mmol), whereafter THF (2 mL) was added. The resultant mixture was stirred in a water bath (35 °C) for few minutes to afford a clear light yellow (slightly greenish-yellow) solution. Upon cooling to room temperature, dry air (12 mL, corresponding to ca. 0.105 mmol of O_2) was added into the lower half of gas phase of this Schlenk flask via syringe through a septum, and excess argon was allowed to leave through an oil trap before the flask was closed. Within minutes, the color of the solution turned deep blue, and formation of dark blue crystals commenced within few hours. The contents were stored undisturbed at room temperature overnight, whereupon the supernatant was decanted, and the solid product was dried in vacuum. Yield: 171 mg (0.29 mmol, 71%) of **3b**. Elemental analysis calculated for $C_{26}H_{21}ClCuN_4O_4Si$ (580.55 g·mol^{-1}): C, 53.79%; H, 3.65%; N, 9.65%; found C, 53.95%; H, 3.96%; N, 9.33%.

Compound **3c** $BnSi(\mu^2\text{-pyO})_4CuCl$ ($C_{27}H_{23}ClCuN_4O_4Si$). Under a dry argon atmosphere, a Schlenk flask (volume ca. 80 mL) was charged with magnetic stirring bar, silane **1c** ($BnSi(pyO)_3$, 390 mg, 0.97 mmol) and CuCl (65 mg, 0.66 mmol), whereafter THF (3 mL) was added. The resultant mixture was briefly stirred at room temperature to afford a clear light yellow (slightly greenish-yellow) solution. Thereafter, dry air (18.5 mL, corresponding to ca. 0.162 mmol of O_2) was added into the lower half of gas phase of this Schlenk flask via syringe through a septum, and excess argon was allowed to leave through an oil trap before the flask was closed. Within minutes, the color of the solution turned deep blue, and formation of yellow crystals of **2c** and of dark blue crystals of **3c** commenced within few hours. The contents were stored undisturbed at room temperature for 4 d to allow for dissolution and reaction of **2c** and final crystallization of **3c**. Thereafter, the supernatant was decanted, and the solid product was washed with THF (1 mL) and dried in vacuum. Yield: 290 mg (0.49 mmol, 74%) of **3c**. Elemental analysis calculated for $C_{27}H_{23}ClCuN_4O_4Si$ (594.58 g·mol^{-1}): C, 54.54%; H, 3.90%; N, 9.42%; found C, 54.44%; H, 3.80%; N, 9.34%.

Compounds $\mathbf{5^2}$ $Ph_2Si(\mu^2\text{-pyO})_2(CuCl)_2(\mu^2\text{-pyO})_2SiPh_2$ ($C_{44}H_{36}Cl_2Cu_2N_4O_4Si_2$) and ($\mathbf{5^4}$)·$(THF)_2$ $Ph_2Si(\mu^2\text{-pyO})_2(CuCl)_4(\mu^2\text{-pyO})_2SiPh_2$·$(THF)_2$ ($C_{52}H_{52}Cl_4Cu_4N_4O_6Si_2$). Under a dry argon atmosphere, a Schlenk flask was charged with magnetic stirring bar, silane **4** (0.308 g, 0.83 mmol) and CuCl (82 mg, 0.83 mmol), whereafter THF (1 mL) was added. The resultant mixture was briefly stirred at room temperature until complete dissolution of CuCl was achieved to afford a light yellow (slightly greenish-yellow) solution, which was connected to another flask with 3 mL of diethyl ether for gas phase diffusion. In the course of ether diffusion, yellow crystals and colorless crystals (of $\mathbf{5^2}$ and ($\mathbf{5^4}$)·$(THF)_2$, respectively) formed simultaneously. Judged by observation, the product mixture contained near equal amounts of the two products. They were suitable for single-crystal X-ray diffraction analysis. In a repeated attempt, using a slight excess of silane **4** to suppress formation of the CuCl-rich by-product ($\mathbf{5^4}$)·$(THF)_2$ (batch size: 1.20 g, 3.24 mmol of **4**; 280 mg, 2.83 mmol of CuCl, 3 mL of THF, 5 mL of diethyl ether), colorless crystals of ($\mathbf{5^4}$)·$(THF)_2$ were obtained exclusively. After 2 d, the supernatant was removed by decantation, the crystals were washed with 2 × 2 mL of a mixture (1:1) of THF and diethyl ether and briefly dried in

vacuum. Yield: 0.88 g (0.687 mmol, 97%) of (**5⁴**)·$(THF)_2$. Elemental analysis indicated loss of solvent during sample preparation, the composition is close to solvent free: Calculated for $C_{44}H_{36}Cl_4Cu_4N_4O_4Si_2$ (1145.01 g·mol^{-1}): C, 46.48%; H, 3.19%; N, 4.93%; found C, 46.07%; H, 3.40%; N, 4.81%. $^{29}Si\{^1H\}$ NMR (CP/MAS): δ_{iso} (ppm) −32.4.

Compound (**5³**)·($CHCl_3$) $Ph_2Si(\mu^2\text{-pyO})_2(CuCl)_3(\mu^2\text{-pyO})_2SiPh_2\cdot(CHCl_3)$ ($C_{45}H_{37}Cl_6Cu_3N_4O_4Si_2$). Under dry argon atmosphere, a Schlenk flask was charged with magnetic stirring bar, silane **4** (0.735 g, 1.98 mmol) and CuCl (180 mg, 1.82 mmol), whereafter chloroform (2 mL) was added. The resultant mixture was briefly stirred at room temperature until complete dissolution of CuCl was achieved to afford a light yellow (slightly greenish-yellow) solution, which was connected to another flask with 5 mL of diethyl ether for gas phase diffusion. During ether diffusion, colorless crystals of (**5³**)·($CHCl_3$) formed. After 1 week, the supernatant was removed by decantation, the crystals were washed with 2 mL of a mixture (1:1) of chloroform and diethyl ether and briefly dried in vacuum. Yield: 0.45 g (0.389 mmol, 64%) of (**5³**)·($CHCl_3$). Elemental analysis indicated loss of solvent during sample preparation, the composition corresponds to chloroform content of 0.4 $CHCl_3$: Calculated for $C_{44}H_{36}Cl_3Cu_3N_4O_4Si_2$ 0.4($CHCl_3$) (1085.70 g·mol^{-1}): C, 49.12%; H, 3.38%; N, 5.16%; found C, 49.05%; H, 3.57%; N, 5.15%. $^{29}Si\{^1H\}$ NMR (CP/MAS): δ_{iso} (ppm) −32.9, −33.5.

4. Conclusions

With the successful syntheses of further Cu(I) complexes of the type RSi(μ^2-pyO)$_3$CuCl (**2b**: R = Ph, **2c**: R = Bn) we have shown that silanes of the type RSi(pyO)$_3$ are suitable tridentate N-donor ligands for complex formation with Cu(I). If R = Allyl, this hydrocarbyl group serves as an alternative ligand site, and complex AllylSi(μ^2-pyO)$_3$CuCl (**2d**) isomerizes to the more stable isomer (κO-pyO)Si(μ^2-pyO)$_2$(μ^2-Allyl)CuCl (**2d′**). The inherent allyl group activation by Cu(I) coordination of the latter asks for further exploration of **2d′** as an allyl transfer reagent. As shown by ^{29}Si and ^{63}Cu solid-state NMR spectroscopy for the couple of **2c** and **2d′**, the switch from (pyO)$_3$- to (pyO)$_2$(Allyl)-Cu-coordination causes noticeable differences in the ^{29}Si isotropic chemical shift and in the ^{63}Cu chemical shift anisotropy.

A deliberate synthesis of paddlewheel compounds of the type RSi(μ^2-pyO)$_4$CuCl (**3a**: R = Me, **3b**: R = Ph, **3c**: R = Bn) has been established. The use of dry air (in stoichiometric ratio with respect to oxygen contained therein) and of excess of the respective silane RSi(pyO)$_3$ to account for pyO-group delivery and oxide trapping proved successful. The corresponding allyl compound **3d** (AllylSi(μ^2-pyO)$_4$CuCl), however, was obtained in small amounts only.

Crystal structure analyses of the series **2a**–**2d** and **3a**–**3d** indicated that the Cu···Si distance is not significantly responsive to the Si-bound hydrocarbyl group in series **2**, whereas a trend of slight Si···Cu approach with increasing electronegativity of R is indicated in series **3**. Especially in the series **2**, the Cu···Si atom distances of ca. 3.2 Å should be interpreted as a close spatial proximity without noticeable effects of Si hypercoordination. Computational comparison of the ^{29}Si NMR shifts of PhSi(pyO)$_3$ (**1b**), PhSi(μ^2-pyO)$_3$CuCl (**2b**) and hypothetical compound PhSi(μ^2-pyO)$_3$LiCl (**2bLi**) indicated that the upfield shift of the Si NMR signal in compounds **2** relative to those of the corresponding silane **1** mainly arises from polarization through coordination of a cation in the (pyO)$_3$ clamp, not necessarily from lone pair donation of this cation toward Si.

In solution, the ligands in compounds of the type **2** are very mobile, even in the absence of competing donor arms (such as Allyl) their ^{1}H and ^{13}C NMR spectra exhibit signs of exchange processes in $CDCl_3$ solution (broad signals of pyO-based H and C atoms). Upon replacing one of the three pyO buttresses by a non-coordinating group, i.e., going to silane $Ph_2Si(pyO)_2$ (**4**), CuCl-coordination of such a silane involves Cu(μ^2-Cl)$_2$Cu bridging. The variety of ladder-type (CuCl)$_n$-complexes obtained (with n = 2, 3, 4 for compounds **5²**, **5³** and **5⁴**, respectively) in spite of using compound **4** in excess demonstrates the preference given to this Cu(μ^2-Cl)$_2$Cu coordination mode and points at the challenges (in

deliberate syntheses and isolation and characterization of pure products) arising therefrom for further studies.

Supplementary Materials: The following supporting information can be downloaded at: https://www.mdpi.com/article/10.3390/inorganics11010002/s1, Crystallographic data for the compounds reported in this paper (in CIF format) and a document containing the following: Details of syntheses and NMR spectroscopic data of $BnSi(pyO)_3$ (**1c**) and $AllylSi(pyO)_3$ (**1d**); graphics of molecular structures of $BnSi(pyO)_3$ (**1c**) and $AllylSi(pyO)_3$ (**1d**) in their crystal structures (Figures S1 and S2) and selected bond lengths and angles (Tables S1–S4); graphics of solution state NMR spectra (^1H, $^{13}C\{^1H\}$ and $^{29}Si\{^1H\}$) of $CDCl_3$ solutions of compounds **1c**, **1d**, $(\mathbf{2b})_2\cdot(THF)$, **2c**, **2d′**, $(\mathbf{5^3})\cdot(CHCl_3)$ and $(\mathbf{5^4})\cdot(THF)_2$ (Figures S3–S23); graphics of ^{29}Si CP/MAS NMR spectra of $(\mathbf{2b})_2\cdot(THF)$, **2c**, **2d′**, $(\mathbf{5^3})\cdot(CHCl_3)$ and $(\mathbf{5^4})\cdot(THF)_2$ (Figures S24–S29); graphical representation of the NEB scan of the interconversion of isomers **2d**, **2d′** (Figure S30); graphics of optimized molecular structures and total energies (Figures S31–S33) as well as atomic coordinates (Tables S5–S7) of compounds **2d**, **2d′** and the transition state (**TS**) of their interconversion; graphics of optimized molecular structures and total energies (Figures S34–S37) as well as atomic coordinates (Tables S8–S11) of tetramethylsilane and of compounds **1b**, **2b**, **2bLi** which were used for calculation of their ^{29}Si NMR shifts.

Author Contributions: Conceptualization, J.W.; investigation, A.S., R.G., E.B. and J.W.; writing—original draft preparation, J.W.; writing—review and editing, R.G., E.B. and J.W.; visualization, R.G. and J.W.; supervision, J.W. All authors have read and agreed to the published version of the manuscript.

Funding: The authors are grateful for computing time at the High-Performance Computing Cluster at TU Bergakademie Freiberg, which was funded by Deutsche Forschungsgemeinschaft (DFG)—397252409.

Data Availability Statement: Not applicable.

Acknowledgments: The authors are grateful to the students Sara Braun and Paul Daßler for the syntheses of some samples of **1c**, **1d** and **2c**, to Beate Kutzner (TU Bergakademie Freiberg, Institut für Anorganische Chemie) for solution NMR service and to Franziska Gründler and Mareike Weigel (TU Bergakademie Freiberg, Institut für Anorganische Chemie) for elemental microanalysis service.

Conflicts of Interest: The authors declare no conflict of interest.

Appendix A

Table A1. Crystallographic data from data collection and refinement for **1c**, **1d** and $(\mathbf{2b})_2$ (THF).

Parameter	1c	1d [1]	$(\mathbf{2b})_2$ (THF)
Formula	$C_{22}H_{19}N_3O_3Si$	$C_{18}H_{17}N_3S_3Si$	$C_{46}H_{42}Cl_2Cu_2N_6O_7Si_2$
M_r	401.49	351.43	1045.04
T(K)	180(2)	180(2)	200(2)
λ(Å)	0.71073	0.71073	0.71073
Crystal system	monoclinic	triclinic	monoclinic
Space group	$P2_1/c$	$P\bar{1}$	$P2_1/n$
a(Å)	10.6121(6)	9.7675(8)	9.1764(4)
b(Å)	17.1874(9)	10.6315(8)	18.4453(10)
c(Å)	11.2970(6)	17.7868(16)	13.3241(5)
α(°)	90	78.951(6)	90
β(°)	92.385(4)	88.972(7)	91.991(3)
γ(°)	90	77.779(6)	90
V(Å^3)	2058.72(19)	1771.2(3)	2253.89(18)
Z	4	4	2
ρ_{calc}(g·cm^{-1})	1.30	1.32	1.54
$\mu_{MoK\alpha}$ (mm^{-1})	0.1	0.2	1.2
F(000)	840	736	1072
θ_{max}(°), R_{int}	28.0, 0.0309	25.0, 0.0560	28.0, 0.0395
Completeness	99.9%	99.8%	99.9%
Reflns collected	24,896	16,879	23,599

Table A1. *Cont.*

Parameter	1c	1d [1]	$(2b)_2$ (THF)
Reflns unique	4961	4242	5437
Restraints	0	20	4
Parameters	263	477	316
GoF	1.118	1.025	1.068
$R1$, $wR2$ [$I > 2\sigma(I)$]	0.0423, 0.1032	0.0435, 0.0905	0.0341, 0.0770
$R1$, $wR2$ (all data)	0.0613, 0.1176	0.0794, 0.1011	0.0507, 0.0848
Largest peak/hole (e·Å^{-3})	0.28, −0.36	0.19, −0.26	0.39, −0.37

[1] The asymmetric unit consists of two molecules of this compound. Both molecules feature disordered allyl groups, which were refined with site occupancies of 0.917(5), 0.083(5) and 0.750(8), 0.260(8) for molecule 1 and 2, respectively.

Table A2. Crystallographic data from data collection and refinement for **2c**, **2d** and **2d′**.

Parameter	2c [1]	2d [2]	2d′
Formula	$C_{22}H_{19}ClCuN_3O_3Si$	$C_{18}H_{17}ClCuN_3O_3Si$	$C_{18}H_{17}ClCuN_3O_3Si$
M_r	500.48	450.42	450.42
T(K)	200(2)	200(2)	180(2)
λ(Å)	0.71073	0.71073	0.71073
Crystal system	orthorhombic	monoclinic	triclinic
Space group	$Pca2_1$	$P2_1/c$	$P\bar{1}$
a(Å)	15.3617(7)	9.0369(2)	8.7413(3)
b(Å)	8.6072(5)	23.5711(6)	10.4028(3)
c(Å)	16.3936(7)	9.6583(2)	10.7168(3)
α(°)	90	90	80.052(3)
β(°)	90	108.839(2)	80.903(2)
γ(°)	90	90	89.273(3)
V(Å^3)	2167.58(18)	1947.10(8)	947.69(5)
Z	4	4	2
ρ_{calc}(g·cm^{-1})	1.53	1.54	1.58
$\mu_{MoK\alpha}$ (mm^{-1})	1.2	1.3	1.4
F(000)	1024	920	460
θ_{max}(°), R_{int}	28.0, 0.0273	28.0, 0.0375	28.0, 0.0299
Completeness	99.9%	100%	100%
Reflns collected	20,601	32,981	19,166
Reflns unique	5100	4701	4570
Restraints	1	27	0
Parameters	280	285	244
GoF	1.087	1.081	1.101
$R1$, $wR2$ [$I > 2\sigma(I)$]	0.0235, 0.0557	0.0336, 0.0790	0.0303, 0.0732
$R1$, $wR2$ (all data)	0.0276, 0.0583	0.0414, 0.0826	0.0353, 0.0753
Largest peak/hole (e·Å^{-3})	0.22, −0.24	0.51, −0.32	0.31, −0.43

[1] The absolute structure parameter χ_{Flack} of this non-centrosymmetric structure refined to −0.010(5). [2] The allyl group of this compound is disordered over two positions, and this disorder causes a disorder of the $Si(pyO)_3$ moiety. Thus, except for the CuCl moiety, the molecule has been refined disordered over two sites with site occupancies 0.901(4) and 0.099(4). For the sake of a stable refinement, the pyridine rings of the part of low occupancy were included in the refinement as ideal hexagons (using the AFIX66 instruction).

Table A3. Crystallographic data from data collection and refinement for **3b**, **3c** and **3d**.

Parameter	3b	3c	3d [1]
Formula	$C_{26}H_{21}ClCuN_4O_4Si$	$C_{27}H_{23}ClCuN_4O_4Si$	$C_{23}H_{21}ClCuN_4O_4Si$
M_r	580.55	594.57	544.52
T(K)	200(2)	200(2)	200(2)
λ(Å)	0.71073	0.71073	0.71073
Crystal system	orthorhombic	monoclinic	monoclinic

Table A3. *Cont.*

Parameter	3b	3c	3d [1]
Space group	*Pbca*	$P2_1/c$	$P2_1/c$
a(Å)	15.7556(8)	15.8215(9)	15.2140(3)
b(Å)	18.2565(7)	9.8221(4)	9.6459(2)
c(Å)	17.2013(6)	17.4885(10)	17.0865(3)
α(°)	90	90	90
β(°)	90	109.961(4)	108.677(1)
γ(°)	90	90	90
V(Å^3)	4947.8(4)	2554.5(2)	2375.44(8)
Z	8	4	4
ρ_{calc}(g·cm^{-1})	1.56	1.55	1.52
$\mu_{MoK\alpha}$ (mm^{-1})	1.1	1.0	1.1
F(000)	2376	1220	1116
θ_{max}(°), R_{int}	28.0, 0.0550	26.0, 0.0312	26.0, 0.0677
Completeness	99.6%	99.8%	100%
Reflns collected	26,190	26,505	33,151
Reflns unique	5951	5012	4670
Restraints	0	0	2
Parameters	334	343	326
GoF	1.011	1.081	1.075
$R1$, $wR2$ [$I > 2\sigma(I)$]	0.0356, 0.0787	0.0291, 0.0704	0.0367, 0.0769
$R1$, $wR2$ (all data)	0.0656, 0.0877	0.0412, 0.0747	0.0517, 0.0817
Largest peak/hole (e·Å^{-3})	0.48, −0.61	0.38, −0.41	0.31, −0.44

[1] The allyl group of this compound is disordered over two positions and has been refined with site occupancies 0.685(12) and 0.315(12).

Table A4. Crystallographic data from data collection and refinement for **5^2**, (**5^4**)·(THF)$_2$ and (**5^3**)·($CHCl_3$).

Parameter	5^2	(5^4) (THF)$_2$ [1]	(5^3) ($CHCl_3$) [2]
Formula	$C_{44}H_{36}Cl_2Cu_2N_4O_4Si_2$	$C_{52}H_{52}Cl_4Cu_4N_4O_6Si_2$	$C_{45}H_{37}Cl_6Cu_3N_4O_4Si_2$
M_r	938.93	1281.11	1157.28
T(K)	180(2)	180(2)	180(2)
λ(Å)	0.71073	0.71073	0.71073
Crystal system	triclinic	triclinic	monoclinic
Space group	$P\bar{1}$	$P\bar{1}$	Pn
a(Å)	9.6434(6)	9.6236(3)	8.9766(2)
b(Å)	10.4351(6)	12.6110(4)	19.8415(3)
c(Å)	12.0659(7)	12.8592(4)	13.5256(3)
α(°)	100.595(5)	110.726(2)	90
β(°)	110.075(5)	107.692(2)	92.846(2)
γ(°)	106.546(5)	98.836(2)	90
V(Å^3)	1038.34(12)	1329.53(8)	2406.06(8)
Z	1	1	2
ρ_{calc}(g·cm^{-1})	1.50	1.60	1.60
$\mu_{MoK\alpha}$ (mm^{-1})	1.3	1.9	1.7
F(000)	480	652	1168
θ_{max}(°), R_{int}	28.0, 0.0293	28.0, 0.0387	28.0, 0.0547
Completeness	100%	100%	99.9%
Reflns collected	16,743	25,647	52,253
Reflns unique	5010	6424	11,597
Restraints	0	0	32
Parameters	262	316	603
GoF	1.072	1.038	1.086
$R1$, $wR2$ [$I > 2\sigma(I)$]	0.0334, 0.0838	0.0346, 0.0833	0.0330, 0.0697

Table A4. *Cont.*

Parameter	5^2	(5^4) $(THF)_2$ [1]	(5^3) $(CHCl_3)$ [2]
*R*1, *wR*2 (all data)	0.0391, 0.0865	0.0469, 0.0876	0.0418, 0.0737
Largest peak/hole (e·Å^{-3})	0.90, −0.45	0.40, −0.48	0.25, −0.46

[1] This structure features two heavy disorders: (1) The $[Ph_2Si(pyO)_2(CuCl)_2]_2$ molecule is located on a crystallographically imposed center of inversion, but the central $(CuCl)_4$ moiety does not adhere to inversion symmetry. Thus, the entire $(CuCl)_4$ moiety was modeled with site occupancy 0.5, and the center of inversion generates its alternative orientation within the peripheral $Ph_2Si(pyO)_2$ clamps. (2) The structure features solvent of crystallization (THF), which was found severely disordered and could not be refined to satisfactory extent. Thus, the data set was treated with SQUEEZE as implemented in PLATON [65–67]. This procedure detected, per unit cell, solvent accessible volume of 271 Å^3 and contributions of 78 electrons therein (in accordance with 80 electrons for the two THF molecules per unit cell, which have been omitted from refinement). [2] The absolute structure parameter χ_{Flack} of this non-centrosymmetric structure refined to −0.004(5). The molecule of solvent of crystallization (chloroform) is disordered and was refined in two positions with site occupancies 0.35(3) and 0.65(3).

References

1. Avent, A.G.; Gehrhus, B.; Hitchcock, P.B.; Lappert, M.F.; Maciejewski, H. Synthesis and characterisation of bis(amino)silylene–nickel(0), –palladium(II), –platinum(0), –platinum(II) and copper(I) complexes. *J. Organomet. Chem.* **2003**, *686*, 321–331. [CrossRef]
2. Paesch, A.N.; Kreyenschmidt, A.-K.; Herbst-Irmer, R.; Stalke, D. Side-Arm Functionalized Silylene Copper(I) Complexes in Catalysis. *Inorg. Chem.* **2019**, *58*, 7000–7009. [CrossRef] [PubMed]
3. Chen, M.; Wang, Y.; Xie, Y.; Wei, P.; Gilliard, R.J., Jr.; Schwartz, N.A.; Schaefer, H.F., III; von Schleyer, R.P.; Robinson, G.H. Dynamic Complexation of Copper(I) Chloride by Carbene-Stabilized Disilicon. *Chem. Eur. J.* **2014**, *20*, 9208–9211. [CrossRef]
4. Gualco, P.; Amgoune, A.; Miqueu, K.; Ladeira, S.; Bourissou, D. A Crystalline σ Complex of Copper. *J. Am. Chem. Soc.* **2011**, *133*, 4257–4259. [CrossRef] [PubMed]
5. Plotzitzka, J.; Kleeberg, C. [(NHC)Cu^I−ER_3] Complexes (ER_3 = $SiMe_2Ph$, $SiPh_3$, $SnMe_3$): From Linear, Mononuclear Complexes to Polynuclear Complexes with Ultrashort Cu^I···Cu^I Distances. *Inorg. Chem.* **2016**, *55*, 4813–4823. [CrossRef] [PubMed]
6. Plotzitzka, J.; Kleeberg, C. [(18-C-6)K][(N≡C)Cu^I−$SiMe_2Ph$], a Potassium Silylcyanocuprate as a Catalyst Model for Silylation Reactions with Silylboranes: Syntheses, Structures, and Catalytic Properties. *Inorg. Chem.* **2017**, *56*, 6671–6680. [CrossRef]
7. Klett, J.; Klinkhammer, K.W.; Niemeyer, M. Ligand Exchange between Arylcopper Compounds and Bis(hypersilyl)tin or Bis(hypersilyl)lead: Synthesis and Characterization of Hypersilylcopper and a Stannanediyl Complex with a Cu−Sn Bond. *Chem. Eur. J.* **1999**, *5*, 2531–2536. [CrossRef]
8. Frogley, B.J.; Hill, A.F.; Sharma, M.; Sinha, A.; Ward, J.S. Semi-bridging σ-silyls as Z-type ligands. *Chem. Commun.* **2020**, *56*, 3532–3535. [CrossRef]
9. Nova, A.; Suh, H.-W.; Schmeier, T.J.; Guard, L.M.; Eisenstein, O.; Hazari, N.; Maseras, F. An Unusual Example of Hypervalent Silicon: A Five-Coordinate Silyl Group Bridging Two Palladium or Nickel Centers through a Nonsymmetrical Four-Center Two-Electron Bond. *Angew. Chem. Int. Ed.* **2014**, *53*, 1103–1108. [CrossRef]
10. Green, M.L.H. A new approach to the formal classification of covalent compounds of the elements. *J. Organomet. Chem.* **1995**, *500*, 127–148. [CrossRef]
11. Chuit, C.; Corriu, R.J.P.; Reye, C.; Young, J.C. Reactivity of Penta- and Hexacoordinate Silicon Compounds and Their Role as Reaction Intermediates. *Chem. Rev.* **1993**, *93*, 1371–1448. [CrossRef]
12. Wagler, J.; Böhme, U.; Kroke, E. Higher Coordinated Molecular Silicon Compounds. *Struct. Bond.* **2014**, *155*, 29–105. [CrossRef]
13. Lemière, G.; Millanvois, A.; Ollivier, C.; Fensterbank, L. A Parisian Vision of the Chemistry of Hypercoordinated Silicon Derivatives. *Chem. Rec.* **2021**, *21*, 1119–1129. [CrossRef] [PubMed]
14. Grobe, J.; Wehmschulte, R.; Krebs, B.; Läge, M. Alternativ-Liganden. XXXII Neue Tetraphosphan-Nickelkomplexe mit Tripod-Liganden des Typs $XM'(OCH_2PMe_2)_n(CH_2CH_2PR_2)_{3-n}$ (M′ = Si, Ge; n = 0–3). *Z. Anorg. Allg. Chem.* **1995**, *621*, 583–596. [CrossRef]
15. Grobe, J.; Krummen, N.; Wehmschulte, R.; Krebs, B.; Läge, M. Alternativ-Liganden. XXXI Nickelcarbonylkomplexe mit Tripod-Liganden des Typs $XM'(OCH_2PMe_2)_n(CH_2CH_2PR_2)_{3-n}$ (M′ = Si, Ge; n = 0–3). *Z. Anorg. Allg. Chem.* **1994**, *620*, 1645–1658. [CrossRef]
16. Grobe, J.; Lütke-Brochtrup, K.; Krebs, B.; Läge, M.; Niemeyer, H.-H.; Würthwein, E.-U. Alternativ-Liganden XXXVIII. Neue Versuche zur Synthese von Pd(0)- und Pt(0)-Komplexen des Tripod-Phosphanliganden $FSi(CH_2CH_2PMe_2)_3$. *Z. Naturforsch.* **2007**, *62*, 55–65. [CrossRef]
17. Gualco, P.; Lin, T.-P.; Sircoglou, M.; Mercy, M.; Ladeira, S.; Bouhadir, G.; Pérez, L.M.; Amgoune, A.; Maron, L.; Gabbaï, F.P.; et al. Gold–Silane and Gold–Stannane Complexes: Saturated Molecules as σ-Acceptor Ligands. *Angew. Chem. Int. Ed.* **2009**, *48*, 9892–9895. [CrossRef]
18. Wagler, J.; Brendler, E. Metallasilatranes: Palladium(II) and Platinum(II) as Lone-Pair Donors to Silicon(IV). *Angew. Chem. Int. Ed.* **2010**, *49*, 624–627. [CrossRef]

19. Wahlicht, S.; Brendler, E.; Heine, T.; Zhechkov, L.; Wagler, J. 7-Azaindol-1-yl(organo)silanes and Their $PdCl_2$ Complexes: Pd-Capped Tetrahedral Silicon Coordination Spheres and Paddlewheels with a Pd-Si Axis. *Organometallics* **2014**, *33*, 2479–2488. [CrossRef]
20. Ehrlich, L.; Gericke, R.; Brendler, E.; Wagler, J. (2-Pyridyloxy)silanes as Ligands in Transition Metal Coordination Chemistry. *Inorganics* **2018**, *6*, 119. [CrossRef]
21. Lyssenko, K.A.; Korlyukov, A.A.; Antipin, M.Y.; Knyazev, S.P.; Kirin, V.N.; Alexeev, N.V.; Chernyshev, E.A. The nature of the intramolecular transannular Si···N interaction in crystalline 1-methylsilatrane, as found from X-ray diffraction data. *Mendeleev Commun.* **2000**, *10*, 88–90. [CrossRef]
22. Párkányi, L.; Simon, K.; Nagy, J. Crystal and molecular structure of [beta]-1-phenylsilatrane, $C_{12}H_{17}NSi$. *Acta Crystallogr. B* **1974**, *30*, 2328–2332. [CrossRef]
23. Párkányi, L.; Nagy, J.; Simon, K. Crystal and molecular structures of γ-1-phenylsilatrane: Some structural features of silatranes. *J. Organomet. Chem.* **1975**, *101*, 11–18. [CrossRef]
24. White, J.M.; Jones, S. Low-temperature structure of allyl silatrane. *Acta Crystallogr. C* **1999**, *55*, 962–963. [CrossRef]
25. Kuß, S.; Brendler, E.; Wagler, J. Molecular Structures of the Pyridine-2-olates Ph*E*$(pyO)_3$ (*E* = Si, Ge, Sn) − [4+3]-Coordination at Si, Ge vs. Heptacoordination at Sn. *Crystals* **2022**, *12*, 1802. [CrossRef]
26. Seidel, A.; Weigel, M.; Ehrlich, L.; Gericke, R.; Brendler, E.; Wagler, J. Molecular Structures of the Silicon Pyridine-2-(thi)olates $Me_3Si(pyX)$, $Me_2Si(pyX)_2$ and $Ph_2Si(pyX)_2$ (py = 2-Pyridyl, X = O, S), and Their Intra- and Intermolecular Ligand Exchange in Solution. *Crystals* **2022**, *12*, 1054. [CrossRef]
27. Okuniewski, A.; Rosiak, D.; Chojnaki, J.; Becker, B. Coordination polymers and molecular structures among complexes of mercury(II) halides with selected 1-benzoylthioureas. *Polyhedron* **2015**, *90*, 47–57. [CrossRef]
28. Dużak, T.; Kinzhybalo, V.; Ślepokura, K.; Olijnyk, V. Tetraallylsilane π−Complexation: Synthesis and Structure of $[Cu_5Cl_5(CH_2{-}CH{=}CH_2)_4Si]$. *Z. Anorg. Allg. Chem.* **2009**, *635*, 2324–2327. [CrossRef]
29. Kamei, T.; Fujita, K.; Itami, K.; Yoshida, J. Copper-Catalyzed Allylation of Carbonyl Derivatives Using Allyl(2-pyridyl)silanes. *Org. Lett.* **2005**, *7*, 4725–4728. [CrossRef]
30. Shi, C.; Xi, X.; Hou, Z.; Liu, E.; Wang, W.; Jin, S.; Wu, Y.; Wu, G. Atomic-Level Characterization of Dynamics of Copper Ions in CuAgSe. *J. Phys. Chem. C* **2016**, *120*, 3229–3234. [CrossRef]
31. Endo, K.; Yamamoto, K.; Deguchi, K.; Matsushita, K. ^{63}Cu High Resolution NMR of Cu(I) Halides in Aqueous Solution and Suspension. *Bull. Chem. Soc. Jpn.* **1987**, *60*, 2803–2807. [CrossRef]
32. Harris, R.K.; Becker, E.D.; Cabral de Menzenes, S.M.; Goodfellow, R.; Granger, P. Nuclear spin properties and conventions for the chemical shift. *Pure Appl. Chem.* **2001**, *73*, 1795–1818. [CrossRef]
33. Sakida, S.; Kato, N.; Kawamoto, Y. ^{63}Cu magic angle spinning (MAS) nuclear magnetic resonance (NMR) study of CuX crystals (X = Cl, Br, and I) and CuX-based glasses (X = Cl, Br, and I). *Mat. Res. Bull.* **2002**, *37*, 2263–2274. [CrossRef]
34. Tang, J.A.; Ellis, B.D.; Warren, T.H.; Hanna, J.V.; Macdonald, C.L.B.; Schurko, R.W. Solid-State ^{63}Cu and ^{65}Cu NMR Spectroscopy of Inorganic and Organometallic Copper(I) Complexes. *J. Am. Chem. Soc.* **2007**, *129*, 13049–13065. [CrossRef]
35. Massiot, D.; Fayon, F.; Capron, M.; King, I.; Le Calvlé, S.; Alonso, B.; Durand, J.-O.; Bujoli, B.; Gan, Z.; Hoatson, G. Modeling one- and two-dimensional Solid State NMR spectra. *Magn. Reson. Chem.* **2002**, *40*, 70–76. [CrossRef]
36. Gericke, R.; Wagler, J. Coordination and Electrochemical Switching on Paddle-Wheel Complexes Containing an As−Ru or a Sb−Ru Axis. *Inorg. Chem.* **2021**, *60*, 18122–18132. [CrossRef]
37. Dattelbaum, A.M.; Martin, J.D. Benzene−Copper(I) Coordination in a Bimetallic Chain Complex. *Inorg. Chem.* **1999**, *38*, 6200–6205. [CrossRef] [PubMed]
38. Dattelbaum, A.M.; Martin, J.D. Benzene and ethylene binding to copper(I)–ziconium(IV) chloride materials: The crystal structure and solid-state reactivity of $((bz)_2Cu)_2Zr_2Cl_{10} \cdot bz$. *Polyhedron* **2006**, *25*, 349–359. [CrossRef]
39. Daly, S.; Haddow, M.F.; Orpen, A.G.; Rolls, G.T.A.; Wass, D.F.; Wingad, R.L. Copper(I) Diphosphine Catalysts for C-N Bond Formation: Synthesis, Structure, and Ligand Effects. *Organometallics* **2008**, *27*, 3196–3202. [CrossRef]
40. Chen, B.-L.; Mok, K.-F.; Ng, S.-C. Synthesis, crystal structures and dynamic NMR studies of novel trinuclear copper(I) halide complexes with 2,5-bis[(diphenylphosphino)-methyl]thiophene. *J. Chem. Soc., Dalton Trans.* **1998**, 2861–2866. [CrossRef]
41. Collins, L.R.; Lowe, J.P.; Mahon, M.F.; Poulten, R.C.; Whittlesey, M.K. Copper Diamidocarbene Complexes: Characterization of Monomeric to Tetrameric Species. *Inorg. Chem.* **2014**, *53*, 2699–2707. [CrossRef] [PubMed]
42. Crestani, M.G.; Manbeck, G.F.; Brennessel, W.W.; McCormick, T.M.; Eisenberg, R. Synthesis and Characterization of Neutral Luminescent Diphosphine Pyrrole- and Indole-Aldimine Copper(I) Complexes. *Inorg. Chem.* **2011**, *50*, 7172–7188. [CrossRef] [PubMed]
43. Köhn, R.D.; Laudo, L.D.; Pan, Z.; Speiser, F.; Kociok-Köhn, G. Triangular tricopper(I) clusters supported by donor-substituted triazacyclohexanes. *Dalton Trans.* **2009**, 4556–4568. [CrossRef] [PubMed]
44. Dyason, J.C.; Healy, P.C.; Engelhardt, L.M.; Pakawatchai, C.; Patrick, V.A.; Raston, C.L.; White, A.H. Lewis-base adducts of Group 1B metal(I) compounds. Part 16. Synthesis, structure, and solid-state phosphorus-31 nuclear magnetic resonance spectra of some novel $[Cu_4X_4L_4]$(X = halogen, L = N, P base) 'cubane' clusters. *J. Chem. Soc. Dalton Trans.* **1985**, *14*, 831–838. [CrossRef]
45. Noor, A.; Shahzad, A.; Khan, E.; Tahir, M.N.; Khan, G.S.; ur Rashid, A.; Said, M. Polynuclear Cu(I) and Ag(I) Complexes of 1,3-Diisobutyl Thiourea, Synthesis, Crystal Structure and Antioxidant Potentials. *Inorganics* **2022**, *10*, 185. [CrossRef]

46. Kämpfe, A.; Brendler, E.; Kroke, E.; Wagler, J. Tp*Cu(I)–CN–SiL2–NC–Cu(I)Tp*—A hexacoordinate Si-complex as connector for redox active metals via π-conjugated ligands. *Dalton Trans.* **2015**, *44*, 4744–4750. [CrossRef]
47. Gericke, R.; Wagler, J. Ruthenium complexes of phosphino derivatives of carboxylic amides: Synthesis and characterization of tridentate P,E_2 and tetradentate P,E_3 (E = N,O) ligands and their reactivity towards [$RuCl_2(PPh_3)_3$]. *Polyhedron* **2017**, *125*, 57–67. [CrossRef]
48. Sheldrick, G.M. *Program for the Solution of Crystal Structures*; SHELXS-97; University of Göttingen: Göttingen, Germany, 1997.
49. Sheldrick, G.M. SHELXT—Integrated space-group and crystal-structure determination. *Acta Crystallogr. A* **2015**, *71*, 3–8. [CrossRef]
50. Sheldrick, G.M. *Program for the Refinement of Crystal Structures*; SHELXL-2014/7; University of Göttingen: Göttingen, Germany, 2014.
51. Sheldrick, G.M. *Program for the Refinement of Crystal Structures*; SHELXL-2018/3; University of Göttingen: Göttingen, Germany, 2018.
52. Sheldrick, G.M. A short history of SHELX. *Acta Crystallogr. A* **2008**, *64*, 112–122. [CrossRef]
53. Farrugia, L.J. ORTEP-3 for windows—A version of ORTEP-III with a graphical user interface (GUI). *J. Appl. Crystallogr.* **1997**, *30*, 565. [CrossRef]
54. Farrugia, L.J. WinGX and ORTEP for Windows: An update. *J. Appl. Crystallogr.* **2012**, *45*, 849–854. [CrossRef]
55. *POV-RAY*, (Version 3.7). Trademark of Persistence of Vision Raytracer Pty. Hallam Oaks Pty. Ltd.: Williamstown, Australia, 1991–2013. Available online: http://www.povray.org/download/(accessed on 28 June 2021).
56. Neese, F. Software update: The ORCA program system—Version 5.0. *WIREs Comput. Mol. Sci.* **2022**, *8*, e1606. [CrossRef]
57. Weigend, F.; Ahlrichs, R. Balanced basis sets of split valence, triple zeta valence and quadruple zeta valence quality for H to Rn: Design and assessment of accuracy. *Phys. Chem. Chem. Phys.* **2005**, *7*, 3297–3305. [CrossRef] [PubMed]
58. Pantazis, D.A.; Neese, F. All-electron basis sets for heavy elements. *WIREs Comput. Mol. Sci.* **2014**, *4*, 363–374. [CrossRef]
59. Van Lenthe, E.; Baerends, E.J.; Snijders, J.G. Relativistic regular two-component Hamiltonians. *J. Chem. Phys.* **1993**, *99*, 4597. [CrossRef]
60. Van Wüllen, C. Molecular density functional calculations in the regular relativistic approximation: Method, application to coinage metal diatomics, hydrides, fluorides and chlorides, and comparison with first-order relativistic calculations. *J. Chem. Phys.* **1998**, *109*, 392. [CrossRef]
61. Grimme, S.; Ehrlich, S.; Goerigk, L. Effect of the damping function in dispersion corrected density functional theory. *J. Comput. Chem.* **2011**, *32*, 1456–1465. [CrossRef]
62. Grimme, S.; Antony, J.; Ehrlich, S.; Krieg, H. A consistent and accurate ab initio parametrization of density functional dispersion correction (DFT-D) for the 94 elements H-Pu. *J. Chem. Phys.* **2010**, *132*, 154104. [CrossRef]
63. Stoychev, G.L.; Auer, A.A.; Neese, F. Automatic Generation of Auxiliary Basis Sets. *J. Chem. Theory Comput.* **2017**, *13*, 554–562. [CrossRef]
64. *Chemcraft*, Version 1.8 (Build 164); 2016. Available online: http://www.chemcraftprog.com/ (accessed on 19 September 2015).
65. Spek, A.L. Single-crystal structure validation with the program PLATON. *J. Appl. Cryst.* **2003**, *36*, 7–13. [CrossRef]
66. Spek, A.L. Structure validation in chemical crystallography. *Acta Crystallogr. D* **2009**, *65*, 148–155. [CrossRef] [PubMed]
67. Spek, A.L. PLATON SQUEEZE: A tool for the calculation of the disordered solvent contribution to the calculated structure factors. *Acta Crystallogr. C* **2015**, *71*, 9–18. [CrossRef] [PubMed]